RESEARCH ARTICLE-MECHANICAL ENGINEERING

# Machining Performance of Inconel 718 Under Dry, MQL, and Nanofluid MQL Conditions: Application of Coconut Oil (Base Fluid) and Multi-walled Carbon Nanotubes as Additives

Subham Sarkar[1] · Saurav Datta[1]

© King Fahd University of Petroleum & Minerals 2020

## Abstract

The present work intends to investigate the application potential of coconut oil, as cutting fluid, during metal machining of a nickel-based superalloy. In doing so, machining performance of *difficult-to-cut* aerospace superalloy Inconel 718 is studied under dry, minimum quantity lubrication (MQL), and nanofluid MQL (NFMQL) using uncoated WC–Co tool, operated at varied cutting speeds. MQL environment is created by supplying *air-oil mist* in which commercially available coconut oil is used as cutting fluid. On the other hand, nanofluid is prepared by dispersing a specific concentration of multi-walled carbon nanotubes within coconut oil. Machining performance as observed in MQL and NFMQL is compared to that of dry machining. The following machining performance indicators are considered herein: cutting force magnitude, tool-tip temperature, and width of flank wear progression. In addition, studies on dominant modes and mechanisms of cutting tool wear, chip morphology (macro/micro), and surface roughness of the machined work part are also carried out. In the purview of machined surface roughness, it is concluded that NFMQL performs better than dry machining and conventional MQL. Flank wear is witnessed more severe during dry machining than MQL/NFMQL. However, beyond 83 m/min cutting speed, conventional MQL outperforms NFMQL (with 0.2 wt% nano-additives concentration) machining, from the viewpoint of flank wear width.

## 1 Research Background

Superalloy (also called high-performance alloy) is the family of alloys which shows excellent high-temperature strength, high corrosion and oxidation resistance, good surface stability, and outstanding resistance toward thermal creep deformation. Inconel 718 is a nickel-based superalloy which consists of a high amount of nickel, chromium, and iron; and a considerable amount of niobium and molybdenum. The presence of niobium age-hardens the alloy, and thus, provides high strength as well as high fatigue resistance. Inconel 718 belongs to the family of heat-resistant superalloy (HRSA); it shows excellent thermal resistance and can retain mechanical properties at elevated temperatures, generally above 700 °C.

These properties make the alloy suitable for diverse applications including turbine engines, cryogenic tankages, various parts of aircrafts, and liquid rockets [1]. Inconel 718 also exhibits excellent welding characteristics such as resistance toward post-weld cracking. The austenitic fcc (face-centered cubic) crystal structure improves the mechanical properties of this alloy [2].

In spite of a wide range of applications, the major drawback of Inconel 718 is its poor machinability. It belongs to the group of *difficult-to-cut* material family [1]. Inconel 718 retains its strength (hot strength) even at extreme temperature conditions. The alloy's strain rate sensitivity and strong work-hardening tendency result in rapid tool wear. The presence of hard carbide particles (highly abrasive in nature) in its microstructure results in abrasion wear of the cutting tool [3]. Low thermal conductivity (~ 15 W/m/K) of Inconel 718 results in excessive cutting zone temperature (up to 1200 °C). The high chemical affinity of Inconel 718 (toward tool materials/Co-binders) leads to diffusion wear

✉ Saurav Datta
sdatta@nitrkl.ac.in

[1] Department of Mechanical Engineering, National Institute of Technology, Rourkela, Odisha 769008, India

[4]. Chip welding, adhesion, notching, and peel off tool material (as pull out) cause altered tool geometry. Due to the high-temperature strength of Inconel 718, a high magnitude of cutting forces is evolved which further causes excessive vibration (chatter) of the machine tool, and finally, disappointing surface quality of the machined work part. Though, conventional dry machining is advantageous due to its cost effectiveness, environment-friendliness, and fulfillment of requirements for occupational health and safety issues [4]; machining, without application of cutting fluid, is always criticized, specifically, when machining *difficult-to-cut* materials. On the contrary, wet machining consumes cutting fluid to ensure better cooling and lubrication effects which in turn improve machining performance. Wet cooling strategies are further classified as follows: flood cooling, minimum quantity lubrication (MQL), and nanofluid MQL (NFMQL).

When machining is executed at lower cutting speeds, cutting zone temperature remains relatively less; flood cooling emerges as an effective solution with enhanced tool life. Coolant provides flushing action by evacuating chips and adds corrosive resistance to the machined part. For higher cutting speeds, at high cutting temperature, cutting fluid, often, gets vaporized and forms a steam barrier which prohibits adequate penetration into the cutting zone [5]. This problem is overcome by supplying highly pressurized jet of coolant which effectively penetrates the cutting zone, creates hydrodynamic wedge at tool-chip/tool-work interfaces, and lifts evolved chips from the tool rake face. Effective penetration of cutting fluid also reduces cutting zone temperature and lowers interfacial friction which leads to a significant increment in tool life. In spite of these advantages, flood cooling possesses harmful environmental impact, and consumption of huge coolant leads to elevated production costs. As a result, the MQL technique appears as a suitable alternative. In MQL, a relatively tiny amount (typically 10–100 ml/h) of cutting fluid is sprayed over the cutting zone along with pressurized air in the form of *air-oil mist* [6, 7]. MQL provides a cost-effective, and environment-friendly solution of cooling/lubrication in machining. In spite of less toxicity, environment-friendliness (biodegradable), and cost-effectiveness, the usage of vegetable oil-based MQL is somewhat restricted due to its poor thermal conductivity [8]. In order to overcome these, the application of nano-sized additives, dispersed within base cutting fluid, is recommended in the literature (called NFMQL).

Nanofluid is prepared by adding (in suitable proportion) nano-sized particles of metals/ceramics/Carbon Nanotubes (CNTs) into the base cutting fluid. The addition of nano-particles into base fluid offers several advantages. *Brownian* motion of nano-sized particles within base cutting fluid enhances the dispersion stability of the resultant cutting fluid. Dispersed nano-particles due to their higher specific surface area, in turn, improves heat transfer coefficients. Thermal

conductivity and wettability of the base fluid can be improved through the addition of nano-particles within the base fluid, at a suitable ratio [9].

Literature provides adequate evidence that NF possesses higher thermal conductivity than base cutting fluid. Yang et al. [10] reported that the addition of Graphene oxide into water significantly enhanced (~48.15%) thermal conductivity of the resultant nanofluid when compared to base fluid (water). Xie et al. [11] also obtained improved thermal conductivity of nanofluids when nano-particles $SiO_2$, $ZnO$, $TiO_2$, $MgO$, and $Al_2O_3$ were added separately to the base fluid (ethylene glycol). MgO-based nanofluid exhibited the highest increment in thermal conductivity (~40.6%). Yang et al. [12] obtained improved thermal property of nanofluid (MWCNTs dispersed PAO6) when compared to the base fluid.

In this context, the present work attempts to investigate the machinability of Inconel 718 under NFMQL condition. Inconel 718, being *difficult-to-cut*; its machining response is still a controversy. In order to overcome the dry machining challenges of Inconel 718, the application feasibility of NFMQL machining is explored. Nanofluid is prepared by dispersing Multi-Walled Carbon Nanotubes (MWCNTs) into the base fluid (coconut oil). The performance of NFMQL is further compared with conventional MQL as well as dry machining. The work studies the effects of cutting speed on cutting force, tool-tip temperature, width of flank wear, dominant tool wear mechanisms, chip morphology, and machined surface roughness. In addition, the work determines a feasible range of cutting speed for the effective application of NFMQL.

## 2 Literature Review

Inconel 718 is widely applied in the aerospace, automotive, and defense industries. Specific examples of products made by Inconel 718 are nuts and bolts, pipe flanges, threaded fittings, screws, socket weld fittings, gas turbine blades, etc. These products while being manufactured, often, require machining operation(s) to be executed. However, Inconel 718 is known as *difficult-to-machine*. This is because when machined, this alloy encounters several challenges. Thus, the machinability of Inconel 718 is said to be very poor. Dry machining is not at all recommended for Inconel 718. In order to improve the machining performance of Inconel 718, the application potential of adapting MQL/NFMQL strategies is studied. The following sections present *state-of-art* on past research carried out toward evaluating machinability of Inconel 718.

Zhuang et al. [1] investigated mechanism tool wear during dry machining of Inconel 718 with a ceramic tool insert. Authors predicted notch wear depth into consideration with

work-hardened layer formation due to plastic deformation. Choudhury and Baradie [13] conducted dry turning experiments on Inconel 718 with cemented carbide (uncoated and coated) tools. The authors studied the influence of machining variables (cutting velocity, feed rate, and depth-of-cut) on cutting forces and tool life. The use of a coated tool was found justified for deeper depth-of-cut (more than 1 mm). Sharman et al. [5] examined the effects of jet pressure and the direction of cutting fluid jet on surface integrity of finish-turned Inconel 718. It was reported that ultra-high-pressurized cutting fluid caused a significant reduction in tensile residual stresses. Rahman et al. [14] investigated on machinability characteristics of Inconel 718 using two cutting inserts: Physical Vapor Deposition (PVD) TiN-coated and Chemical Vapor Deposition (CVD) TiN-coated carbide inserts. Machined surface roughness, tool flank wear, and cutting forces were considered as machinability assessment criteria. It was experienced that side-cutting edge angle along with cutting velocity, and feed rate played a pivotal role toward determining tool life. Kitagawa et al. [15] worked on the thermal aspects of High Speed Machining (HSM) of the Inconel 718 workpiece. Cutting zone temperature and tool wear were studied up to cutting velocity of 600 m/min. Results revealed that the abrasion mechanism promoted notch wear of the cutting tool. Ezugwu and Bonney [16] conducted machining experiments on Inconel 718 by PVD TiCN/Al$_2$O$_3$/TiN-coated carbide tool up to a cutting velocity of 50 m/min. The authors varied the pressure of the cutting fluid from conventional value to high-pressure values (up to 203 bar). High-pressure supply of cutting fluid improved machined surface finish and caused a significant increment in tool life (~ 740%). Altin et al. [17] examined the influence of cutting velocity on tool wear as well as tool life while turning of Inconel 718 with the ceramic tool of different geometrical shapes (round type and square type), under pressurized cutting fluid (water) supply. It was experienced that a square-shaped tool experienced minimal flank wear at a lower range of cutting velocity. On the contrary, a higher range of cutting velocity caused lesser flank wear for a round-type insert. Kaynak [18] conducted cryogenic machining of Inconel 718 using uncoated carbide insert; aspects of machinability were compared with dry machining and MQL. Experimental results showed that dry machining corresponded to higher cutting forces. At the beginning of machining, a lesser extent of Built-Up-Edge (BUE) was formed under MQL when compared to dry well as cryogenic cooling environments. MQL caused tool wear rate approximately similar to that of cryogenic cooling (up to 150 s machining duration); afterward, increased tool wear rate was noticed under MQL, and finally, wear rate appeared similar to that of dry machining. Kamata and Obikawa [6] conducted MQL turning experiments on Inconel 718 with various coated carbide tools at cutting velocity range ~ 60–90 m/min. Machining performance was

compared to that of dry and wet machining. Tool life and surface finish were considered as machinability evaluation criteria. TiCN/Al$_2$O$_3$/TiN-coated insert outperformed PVD TiN/AlN superlattice, and PVD TiAlN-coated inserts. It was reported that carrier gas played a significant role toward providing cooling effects during machining. In addition, a better-machined surface finish, as obtained under MQL, was due to roughing of worn-out tool flank face. Obikawa et al. [7] performed MQL finish turning on Inconel 718 at the micro-liter lubrication range (flow rate < 1 ml/h) with coated carbide tool. The authors applied especially designed cover-type nozzles for providing a tiny volume of concentrated lubricant flow into the cutting zone. Machining efficiency was interpreted in terms of tool life. Results indicated that concentrated flow of lubricants enhanced performance as well as the effectiveness of the MQL process. Zhang et al. [19] studied aspects of tool wear and cutting forces during end milling of Inconel 718 with coated tools under dry and vegetable oil (Bescut 173)-based MQL environment. 1.57 times increment in tool life was experienced under MQL than dry cutting. It was reported that MQL attributed to lower cutting forces which further caused friction at tool-chip/tool-work interfaces. MQL also caused lower tool wear due to superior cooling and lubrication provided by the cutting fluid. Rahim and Sasahara [20] conducted MQL drilling experiments on Inconel 718 with AlTiN-coated carbide drills; with synthetic ester, and palm oil (as cutting fluids). Machining performance was evaluated in the purview of the quality of the machined surface and microhardness. The high viscosity of palm oil resulted in efficient cooling and lubrication effects; palm oil emerged as superior within the entire range of cutting velocity and feed rate experimented.

Chetan et al. [9] performed NFMQL turning experiments on Nimonic 90 superalloy with CVD multilayered TiN–MT–TiCN–Al$_2$O$_3$–TiN-coated WC–Co tool. The authors prepared nanofluids by dispersing silver nanoparticles and Al$_2$O$_3$ powder within water. Lower cutting force, reduced degree of chip curling, and lower tool wear rate were observed while machining with alumina-based nanofluid. This was due to the narrower contact angle, enhanced spreadability, and smaller droplet size of the resultant cutting fluid (than base fluid). Behera et al. [21] conducted turning experiments on Inconel 718 with coated carbide tool under MQL, NFMQL, pressurized coolant jet supply, and cryogenic cooling. Cutting force and tool wear were found significantly truncated under NFMQL. In contrast, better surface finish, lesser cutting temperature, and lower residual stress were obtained under cryogenic cooling. Hegab and Kishawy [22] studied performances of MWCNTs and alumina-gamma particles-based nanofluids (vegetable oil as base fluid), respectively, during machining of Inconel 718. Machining performance was evaluated in terms of machined surface roughness and consumed energy in consid-

eration with varied cutting velocity, feed, and concentration of nano-additives. It was experienced that MWCNTs-based nanofluid outperformed alumina-based nanofluid. Hegab et al. [23] conducted NFMQL turning experiments on Inconel 718 by considering two different nanofluids: (a) MWCNTs dispersed into vegetable oil and (b) alumina-gamma nano-particles added to vegetable oil. Machining performance was studied in the purview of tool wear and chip morphology. It was observed that NFMQL outperformed traditional MQL. In addition, MWCNTs-based nanofluid exhibited better performance than alumina-based nanofluid. Vasu and Reddy [24] investigated the machining behavior of Inconel 600 with coated carbide tool under dry, MQL, and NFMQL conditions, respectively. Nanofluid was prepared by dispersing alumina nano-particles at varied concentrations: 4% and 6% (by volume) with vegetable oil. Experimental results revealed that the addition of alumina nano-particles into base cutting fluid enhanced the extent of heat dissipation from the cutting zone, and thereby, improved the surface finish of the machined work part. On the other hand, NFMQL significantly reduced cutting force and tool wear. Superior machining performance was experienced for NFMQL with a 6% alumina concentration. Yıldırım et al. [25] performed dry, MQL, and NFMQL turning experiments on Inconel 625 with coated cemented carbide inserts. hBN nano-particles (concentration: 0.5% and 1%, by volume) dispersed into ester-based base cutting fluid was used as nanofluid. It was evidenced that 0.5% concentration of nano-additives caused consequential increment (~105.9%) in tool life as well as reduction (~43%) in tool wear than dry cutting. Shuang et al. [26, 27] studied the performance of graphene oxide-based nanofluid on the machinability of Ti–6Al–4V.

The literature survey depicts that the substantial volume of work is already documented which focuses on machining, and machinability aspects of Inconel 718 under dry, conventional MQL as well as NFMQL conditions. The application potential of biodegradable vegetable oil (as base cutting fluid) over mineral and synthetic oil is well-understood. The application of coconut oil, as metal working fluid, is already reported in the literature [28–32]; however, such applications are limited to MQL/NFMQL machining of AISI 304/1040 Stainless Steel (SS), mild steel, and cast iron workpieces. Machinability of *difficult-to-material* like Inconel 718 is rarely attempted earlier. In comparison to previous studies, the present work is different in the purview of the composition of cutting fluid, type of nano-additives (dispersed within coconut oil) for preparing nanofluid, concentration of nano-additives, machining parameters, and machinability criteria. For example, Wickramasinghe et al. [28] prepared nanofluid by mixing water with white coconut oil (as base oil), and food-grade additives (as surfactants). The authors considered machined surface roughness and temperature of the tool surface as machinability evaluation criteria. Perera

et al. [29] used white coconut oil as base fluid and considered machined surface roughness as a machining performance index associated with cutting fluid application. Vardhaman et al. [30] studied the effect of cutting lubricants on tool wear, friction coefficient, surface quality, and chip morphology during turning of AISI 1040 steel under different MQL conditions using water-miscible fluid and coconut oil, respectively. Vamsi Krishna et al. [31] studied the application feasibility of boric acid solid lubricant suspensions added to coconut oil (as nanofluid) when machining AISI 1040 steel. The authors considered cutting tool temperature, average tool flank wear, and surface roughness of the machined work part as machinability criteria. Padmini et al. [32] formulated nanofluid using dispersions of nano-molybdenum disulfide ($nMoS_2$) in coconut (CC) oil. The authors concluded that cutting force, temperature, tool wear, and surface roughness were approximately reduced by 37%, 21%, 44%, and 39% respectively, by using CC+ $nMoS_2$ when compared to dry machining.

During metal machining, cutting fluids serve several functions: cool tool and workpiece, reduce friction, protect workpiece against rusting, prevent the formation of (BUEs), evacuate chips from the cutting zone, and improve the surface finish. The choice of a cutting fluid depends on many complex interactions including the machinability of the work material; the severity of the operation; the cutting tool material; metallurgical, chemical, and human compatibility; fluid properties, reliability, and stability; and finally cost. Coconut oil is being used as one of the cutting fluids because of its higher thermal conductivity, and oxidative stability. In addition, coconut oil has abundant availability. It ensures cost economy. According to Xavior and Adithan [33], coconut oil is explored as a cutting fluid because of its thermal and oxidative stability which is comparable to other vegetable-based cutting fluids utilized in machining industries. MWCNTs are selected as additives to utilize advantages of outstanding thermal conductivity, high strength as well as aspect ratio (nano-sized rolled structure) which, in turn, improve *thermophysical*, and *tribological* properties of the resultant cutting fluid. In contrast to the published literature, apart from tool wear and machined surface finish, the present work also includes a detailed study on quantitative features of chip's micro-morphology including equivalent chip thickness, chip segmentation spacing, segmentation frequency, shear angle, saw-tooth included angle, and microhardness. Chip micro-hardness is further correlated with strain rate. Measured chip's micro-morphological data, obtained thereof, are correlated to that of cutting force, tool-tip temperature, and severity of tool wear. The performance of nanofluid lubrication is compared to that of conventional MQL as well as dry machining. The present work also determines a suitable range of cutting speed toward the effective application of NFMQL for machining of Inconel 718.
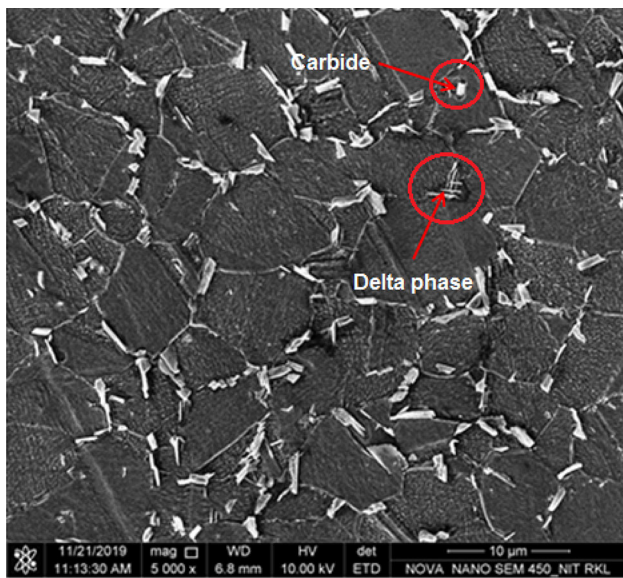
**Fig. 1** Microstructure of *as-received* Inconel 718

**Table 1** Tool geometric features

| Geometric parameter | Value |
| --- | --- |
| Orthogonal rake angle | − 6° |
| Inclination angle | − 6° |
| Orthogonal clearance angle | 6° |
| Principal cutting edge angle | 75° |
| Auxiliary cutting edge angle | 15° |
| Nose radius | 0.8 mm |

# 3 Materials and Methods

A round bar (Ø57 mm) of Inconel 718 is used as a workpiece. Chemical composition and salient properties of Inconel 718 can well be articulated from the literature [16]. The microstructure of *as-received* Inconel 718 work material is exhibited in Fig. 1. The microstructure is composed of Ni-rich $\gamma$ solid solution matrix with some precipitates. The presence of $\delta$ phase ($Ni_3Nb$) is prominently visible (needle-structured appearance) which precipitates at grain boundaries. Other possible precipitates like TiC, NbC, and TiN are found distributed within the matrix [34].

Uncoated WC–Co insert of grade TTS (P25), ANSI designation SNMG120408, is used herein. The insert is mounted on the PSBNR2020K12 type tool holder (Kennametal, WIDIA). The tool geometry of the insert/tool holder combination is provided in Table 1.

Machining (longitudinal turning) experiments are conducted on a high-speed precision lathe (N26, HMT, India). Machining is carried out under dry (without coolant/lubrication), MQL, and NFMQL environment, respectively. Commercially available coconut oil is used

**Table 2** Constituents of *as-received* MWCNTs

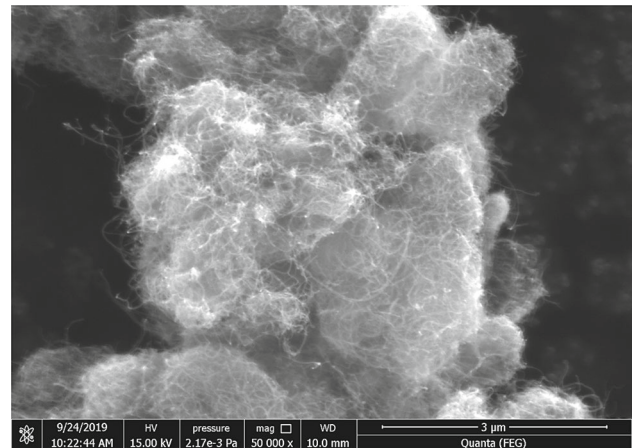| Constituents | Unit | Standard |
| --- | --- | --- |
| Ash content | % | <2% |
| Fe | mg/kg | <4000 |
| Al | mg/kg | <3500 |
| Mo | mg/kg | <800 |



**Fig. 2** FESEM image of MWCNTs

as base cutting fluid. Nanofluid is prepared by dispersing MWCNTs (Diameter: 10–15 nm, Length: 2–10 μm, Purity: >97%, Specific surface area: 250–270 $m^2$/g, Bulk density: 0.06–0.09 g/cc) with the base cutting fluid. Constituents of *as-received* MWCNTs are provided in Table 2. MWCNTs are purchased from Platonic Nanotech Private Limited, Jharkhand, India. FESEM micrograph of *as-received* MWCNTs is provided herein (Fig. 2). MWCNTs are produced by the CVD method. Important properties of MWCNTs are as follows: Thermal conductivity: 6000 W/m/K; Electrical conductivity: 6000 S/cm; Tensile strength: 30–180 GPa; and Young's modulus: 1–2 TPa. Concentration of MWCNTs (within coconut oil) is maintained at 0.2% (by weight).

It is true that an increase in nano-additives concentration (when added to the base fluid) increases the viscosity of the resultant cutting fluid (nanofluid); however, too high concentration leads to poor dispersion stability which, in turn, promotes local agglomeration of the nano-particles, and sedimentation at the bottom of the fluid supply line. Poor dispersion stability adversely affects the performance of the nanofluid. Hence, an optimal concentration needs to be determined by considering nanofluid's thermos-physical properties, dispersion stability, and cost economy.

Coconut oil (also called copra oil) is an edible oil extracted from the *kernel* (or meat) of mature coconuts harvested from the coconut palm. Coconut oil has high levels of saturated fat content; it is prone to slow oxidization and, thus, resists

rancidification. Coconut oil contains a variety of fatty acids like *Lauric* acid, *Myristic* acid, *Caprylic* acid, *Palmitic* acid, *Oleic* acid, *Capric* acid, and *Stearic* acid, with varied fraction percentages. The approximate smoke point of coconut oil is 232 °C, and density: 924.27 kg/m$^3$. In the purview of sustainability issues of vegetable oil, appropriateness of coconut oil was reported in the published literature [35, 36]. Vardhaman et al. [37] reported that coconut oil-based MQL caused lower cutting forces as well as reduced tool wear than soluble oil-based MQL. Senevirathne et al. [38] studied sustainability issues of coconut oil for MQL machining of D2 tool steel. The authors reported that coconut oil caused extended tool life. It was estimated that 82%, 70%, and 44% reduction in tool wear was incurred when using coconut oil-based MQL than dry machining, emulsion flood cooling, and emulsion MQL, respectively. Xavior and Adithan [33] experienced that coconut oil performed better than emulsion, and neat cutting oil toward reducing tool wear and enhancing machined surface quality during turning of austenitic stainless steel. Vamsi Krishna et al. [39] documented better performance of coconut oil-based nano-particle suspensions as compared to SAE-40-based lubricant for turning of AISI 1040 steel. Motivated by this, the present study utilizes coconut oil as base cutting fluid for MQL/NFMQL machining.

MWCNTs, when dispersed within coconut oil (0.2% by weight), causes a significant improvement in viscosity as well as thermal conductivity of the resultant cutting fluid. MWCNTs are dispersed by stirring the oil-additive mixture in a magnetic stirrer (LCMS-6211, Rajendra Electrical Ind. Ltd., India) for 1 h followed by ultrasonication in an ultrasonic bath (Labman, L9174, India), operated at 40 kHz frequency for 2 h duration at temperature, maintained below 40 °C. Procedures for nanofluid preparation are described in Fig. 3.

In MQL setup ("Appendix": Fig. 27), highly compressed air, from a compressor, is supplied through a solenoid-operated on/off valve which is connected to a timer to set the timing (duration) of flow. The pressurized air stream is divided into two parts: one is fed to the oil reservoir to pump the oil in the oil flow line through a filter and a flow control valve (to control flow rate); the other part is fed in the airline through another flow control valve. Oil line, as well as air-line, is connected to a nozzle (2 mm diameter) from which atomized coolant comes out in droplets form. The flow rate of the cutting fluid is maintained at 100 ml/h, at an air pressure of 1 MPa. The nozzle is kept 50 mm apart from the tool cutting edge which makes an angle of 20° with respect to the longitudinal axis of the workpiece.

Turning experiments are carried out in finishing mode; at constant feed = 0.1 mm/rev, and depth-of-cut = 0.3 mm; but at varied cutting speeds: $V_c$ = 64 m/min, $V_c$ = 83 m/min, $V_c$ = 108 m/min, and $V_c$ = 140 m/min. Machining duration is kept constant (~ 40 s) for all four experimental trials under each of the cutting environments: dry, MQL, and NFMQL. Details of the experimental setup are furnished in "Appendix": Fig. 28.

During machining, tangential cutting force (average value), and tool-tip temperature (maximum value) are measured as output responses. Cutting force exerted on the cutting tool is measured by a 4-component force-torque measurement KISTLER 9272 (KISTLER instruments AG, CH-8408 Winterthur, Switzerland) type dynamometer which is connected to a 4-channel charge amplifier of type 5070. Precise temperature recording, exactly at the cutting zone, is indeed very difficult. Therefore, this study records tool-tip temperature as an approximation of cutting zone temperature. Tool-tip temperature is measured by a digital non-contact type infrared thermometer (AR882, Solarman Engineering Project Pvt. Ltd., New Delhi, India). An infrared thermometer can measure the temperature of any specimen surface. The optics sensor of the thermometer emits, transmits, and reflects energy. This energy is focused on the detector where it is collected. The transducer unit of the thermometer converts collected energy to an equivalent measurable form which is measured and finally translates into a temperature reading which is shown in the display unit. In order to enhance the measuring accuracy of the thermometer, the laser pointer must be pointed precisely at the spot. Thus, the tool-tip temperature is measured by focusing the laser beam at the tool-tip. During the prescribed machining duration, the peak temperature reading is noted down.

During experiments, specimen chips are collected, approximately at the midway of the entire machining duration. Chip's macro/micro-morphology, along with worn-out tool edge, is viewed through optical microscopy and scanning electron microscopy. Elemental analysis is performed through EDS. Phases are identified through X-ray Diffraction (XRD) spectroscopy. Vickers's microhardness tester (LM-248AT, Leco Corporation, Michigan, USA) is used for carrying out the chip's microhardness measurements. Surface Roughness (SR), i.e., roughness average ($R_a$) of the machined specimen is measured using Talysurf (Taylor Hobson) in which *cut-off* length of 0.8 mm and *sampling* length of 4 mm are set. For a particular specimen, roughness is measured through five trials; the average of five measurements is taken as the mean surface roughness for analysis purposes.

## 4 Results and Discussion

### 4.1 Cutting Force

Cutting force components are basic indicators of power/energy requirements during machining. The tangential cutting force initially increases with an increase in cutting speed, and reaches the maximum value approximately at $V_c$ = 83 m/min; beyond which it assumes a

**Fig. 3** Procedural steps for preparation of nanofluid
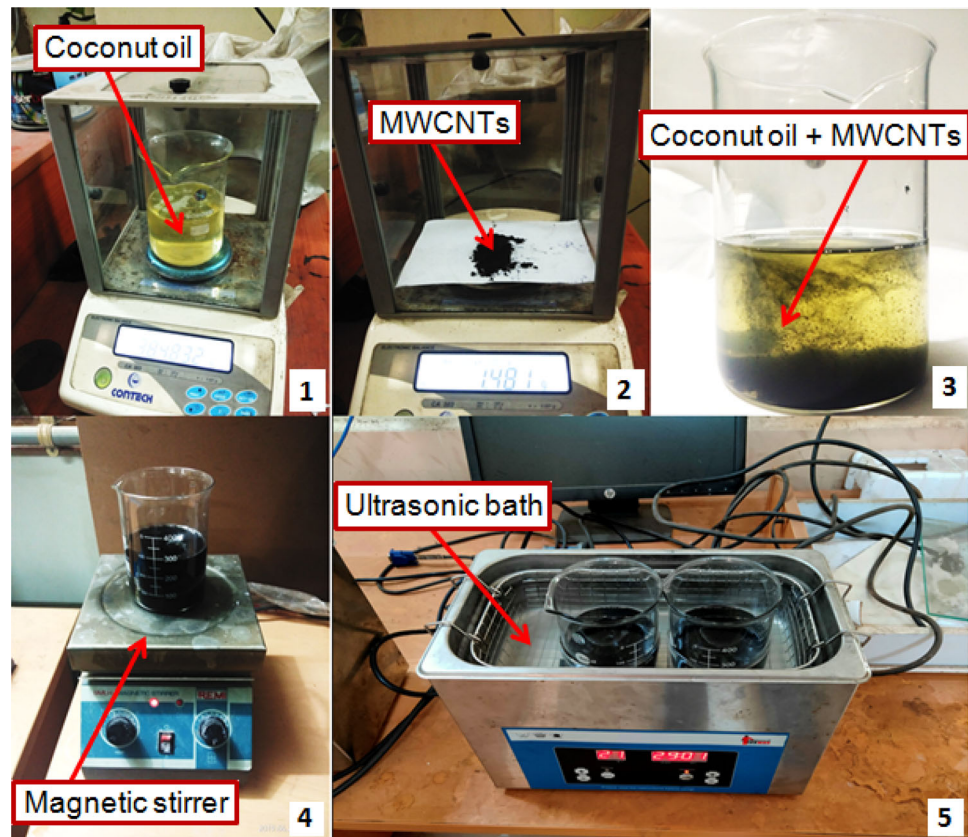


decreasing trend for both dry and MQL machining as shown in Fig. 4a. Strain-hardening of workpiece accompanied by tool blunting, due to plastic deformation, results in the initial increment of cutting force. According to Zhang et al. [19], higher cutting forces are experienced with increased cutting speed due to enhanced flank wear which causes higher friction at tool-work interface and increased area of flak wear (or contact area in wear land). Further reduction in cutting force may be caused due to adequate thermal softening of the workpiece, superseding effects of work-hardening. As a result, machining becomes easier with lower cutting force. As demonstrated by Behera et al. [21], increased chip velocity at higher cutting speeds results in a reduction of frictional effect at the tool-chip interface which further causes a reduction in cutting force. Reduction in chip thickness at higher cutting speed is also attributed to lower cutting forces. The authors further pointed out that work part thermal softening, due to elevated temperatures at higher cutting speeds, is a key factor which plays a significant role for the cutting force to be declined. For MQL, cutting force increases to somewhat up to $V_c = 83$ m/min; afterward, it assumes a slightly declining trend with respect to increased cutting speed.

Investigation reveals that as compared to dry machining, a lesser extent of tool wear along with reduced friction at the tool-chip interface (due to superior cooling capacity and lubricity of cutting fluid) results in truncation of cutting force up to 20% in the case of MQL, and 9–10% for NFMQL, within the experimental domain. Variation of cutting force can also be explained in the purview of mean chip thickness and shear angle, where chip thickness is minimal and shear angle is the maximum for MQL while maximum chip thickness and minimal shear angle are attributed to dry machining. This is further illustrated in later sections. This corresponds to the evolution of lower cutting force under the MQL environment, and the maximum cutting force is attributed to dry machining.

## 4.2 Tool-Tip Temperature

Shearing and plastic deformation in the primary shear zone along with secondary deformation, friction between tool-flowing chip, and rubbing action between tool-work contact surfaces generate immense heat during machining [24]. This heat results in the evolution of high cutting temperatures. Cutting zone temperature plays a significant role in controlling various aspects of machining such as quality of the machined surface, tool wear rate, and tool life. For dry machining and MQL, the tool-tip temperature initially increases with an increase in cutting speed, reaches a maximum value, and afterward starts to decline as shown in Fig. 4b. On the other hand, NFMQL shows a continuous increase in the tool-tip
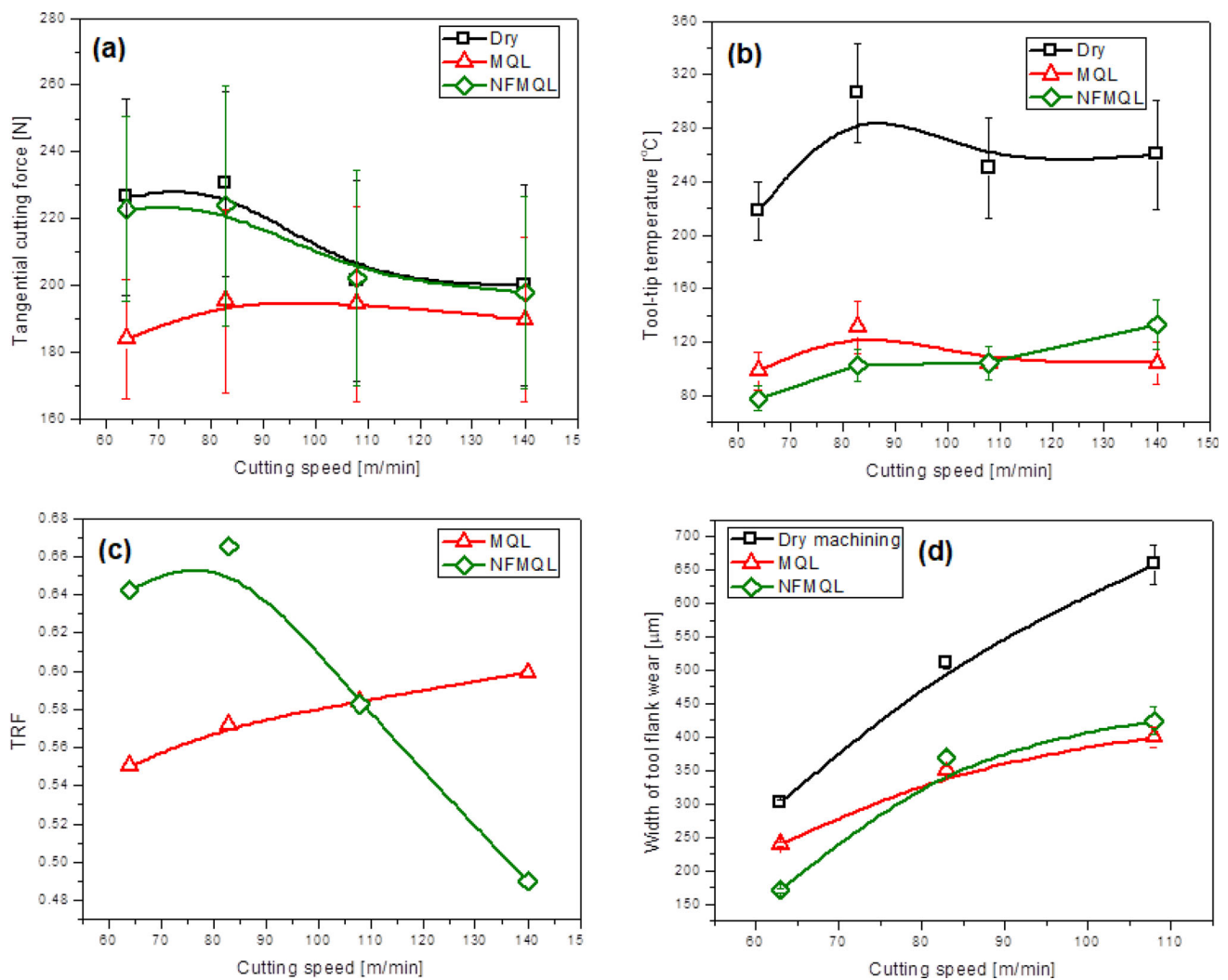
**Fig. 4** Effect of cutting speed on **a** cutting force, **b** tool-tip temperature, **c** TRF, and **d** width of tool flank wear

temperature with increased cutting speed. Initially, with an increase in cutting speed, the workpiece gets strain-hardened which necessitates higher cutting force for metal cutting as shown in Fig. 4a; higher shearing force leads to intense heat generation and, consequently, higher tool-tip temperature. Beyond $V_c = 83$ m/min, the tool-tip temperature is decreased due to a reduction in friction at the tool-chip interface and a higher degree of plastic deformation of the cutting tool which consumes a significant amount of energy. Another reason may be the energy absorbed during welding and the burning of chips. Continuously increasing trend of cutting temperature with respect to cutting speed may be explained by the evolution of cutting heat which appears inadequate for chip welding/burning, and thus, leads to increased tool-tip temperature. The error bars in Fig. 4a shows the combined effect of experimental error accompanied by the instrumental inaccuracy.

Figure 4b also reveals superior cooling and lubrication provided by MQL which substantially reduces the tool-tip

temperature. Tool-tip temperature is further reduced in the case of NFMQL due to enhanced wettability which ensures proper penetration of cutting fluid into the cutting zone and improved thermal conductivity of resultant cutting fluid which causes faster heat dissipation from the cutting zone. MQL environment reduces cutting temperature nearly up to 60% while 67% temperature reduction is evidenced in the case of NFMQL.

In order to evaluate the performance (cooling and lubrication) of cutting fluid with respect to dry machining, the term Temperature Reduction Factor (TRF) is introduced herein. TRF is defined as (for a given set of machining parameters) follows:

$$TRF = \frac{T_d - T_l}{T_d} \tag{1}$$

Here, the term $T_d$ and $T_l$ represent the temperature in dry machining and the temperature under employed lubrication system, respectively, for a given set of machining parameters.

The TRF increases with an increase in cutting speed due to an increase in relative velocity between workpiece and fluid jet in MQL condition which results in quick heat dissipation from the cutting zone (Fig. 4c). On the other hand, due to the improved cooling and lubrication properties of nanofluid, TRF initially increases with an increase in cutting speed and, afterward, declines beyond $V_c = 83$ m/min. This may be due to the impact of centrifugal force, acting at high cutting speed, which results in the separation of nano-particles from the resultant nanofluid.

The exact measurement of cutting zone temperature in real-time machining process is very difficult to achieve [40, 41]. Therefore, in the present work, a non-contact type infrared thermometer is used to measure the approximate cutting zone temperature. The measured value is significantly influenced by the intensity and the wavelength of the beam or the instrumental error accompanied by operators/human error and some operational challenges such as the blocking of the cutting zone by chips or fine droplets of coolant. In order to counter these challenges, the present work proposes a parameter called "Temperature Reduction Factor" (TRF). Temperature reduction factor is a dimensionless parameter in which the generation of heat energy is measured by considering cutting zone temperature under dry machining as a base; and the relative increment or reduction to that with a given cooling strategy.

### 4.3 Width of Tool Flank Wear

Morphology of tool wear (an indicator of tool life) is one of the key aspects for machinability assessment of any work material because it is directly related to evolved of cutting force, power consumed, machined surface quality, and above all, tooling cost in manufacturing. Tool wear is highly influenced by the properties of tool/work material, machining parameters, cooling techniques, and geometry of the tool cutting edge [18, 21]. Optical micrographs display width of flank wear ($V_B$), developed under different machining environments and at varied cutting speeds: $V_c = 64$ m/min, $V_c = 83$ m/min, and $V_c = 108$ m/min (Fig. 5). At the highest cutting speed, i.e., $V_c = 140$ m/min, severe notching is observed at the tool edge; hence, corresponding optical micrographs are excluded.

Quantitative analysis of tool wear is carried out in terms of the width of flank wear progression. Variation of flank wear width is examined at varied cutting speeds and different machining environments through optical micrographs of worn-out tool flank faces (Fig. 4d). With an increase in cutting speed, the width of the flank wear is increased in all machining conditions. At constant cutting speed, a significant reduction in flank wear is observed from dry to MQL or NFMQL. After 40 s machining progression, the width of flank wear still remains within the designed limit according to ISO (1989) which is 0.3 mm (i.e., 300 $\mu$m) [19], for machining under MQL and NFMQL at $V_c = 64$ m/min. It is reported that the failure of carbide tool at higher cutting speeds, during machining of nickel-based superalloys, is affected by thermal softening of tool binder phase (Co) and plastic deformation of tool cutting edge [18]. Under MQL machining, reduction in flank wear width is witnessed due to lower cutting zone temperature caused by adequate cooling and lubrication by the cutting fluid. Lower cutting zone temperature restricts the degree of plastic deformation of the cutting tool. Under NFMQL machining, the introduction of nano-particles further enhances the thermal conductivity of the resultant cutting fluid. This imparts an improved cooling effect. In addition, lower tool-chip/tool-work interfacial friction, due to the *nano-roller*-bearing effect of MWCNTs, results in lower tool wear [9]. Comparative study on flank wear width (between MQL and NFMQL) reveals that up to $V_c = 83$ m/min, the depth of flank wear is lesser for the case of NFMQL due to enhanced *thermophysical* and *tribological* properties of nanofluid which result in higher heat dissipation and lower friction. Beyond $V_c = 83$ m/min, NFMQL corresponds to a higher tool-tip temperature than MQL. This attributes to intense flank wear.

### 4.4 Morphology of Tool Wear

Micrographs of rake and flank face of worn-out tools operated at $V_c = 64$ m/min for 40 s machining duration are arranged in Figs. 6, 7, and 8. A study of wear morphology reveals several tool wear mechanisms including adhesion, abrasion, chip sticking, formation of Built-Up-Layer (BUL), irrespective of dry, MQL, and NFMQL environments. In the case of dry machining, additional attrition mode of tool wear is witnessed. Abrasive wear is the dominant tool wear mode when machining nickel-based superalloys. The abrasive action of hard carbide particles, present in the workpiece, often, erodes tool substrate, and thus, causes abrasion wear [42].

Abrasion marks appear on tool face as scratches or parallel grooves. As demonstrated by Zhu et al. [3], adhesion is similar to cold welding which occurs due to plastic deformation at elevated temperature, and pressure generated during machining. Compressive stresses are induced due to cutting heat generation along with induced temperature gradient. This results in strong bonding between tool-chip and develops a layer of adhered materials over the tool face. According to Akhtar et al. [42], during machining, high stresses result in pressure welding of work material on tool rake/flank face and form BUE/BUL. Such adhered layers are highly unstable and continuously are swept away by flowing chips (as well as a strain-hardened work surface) from the tool face. While dislodging, some tool material also gets eroded or tool chips off. The tool surface becomes rough with cracks and grooves. This wear mechanism is termed as attrition. Extreme chemi-

**Fig. 5** Average width of tool flank wear progression as experienced under different cutting conditions: dry, MQL, and NFMQL
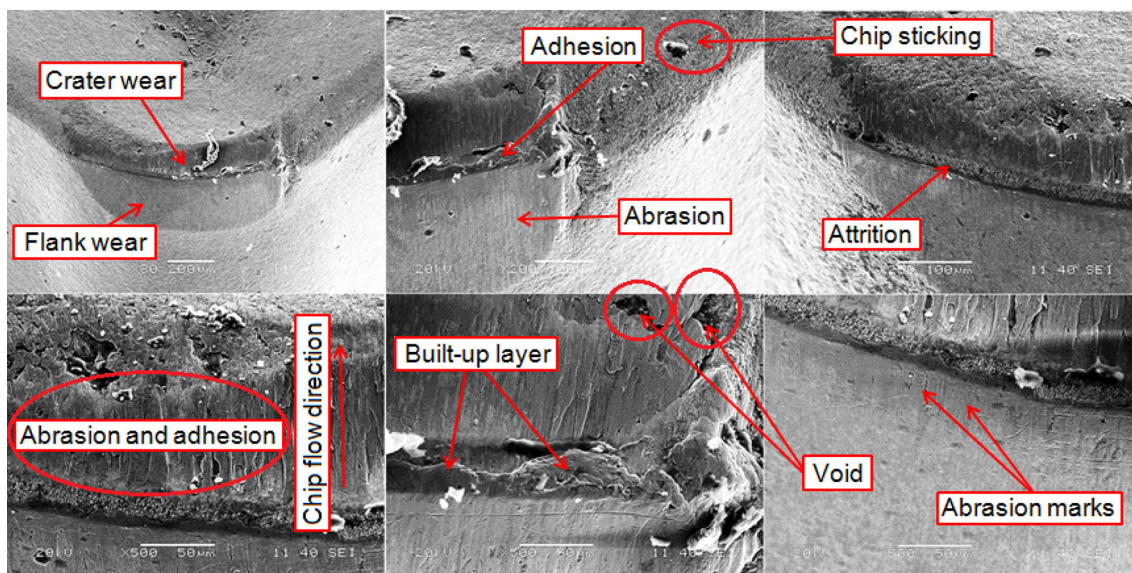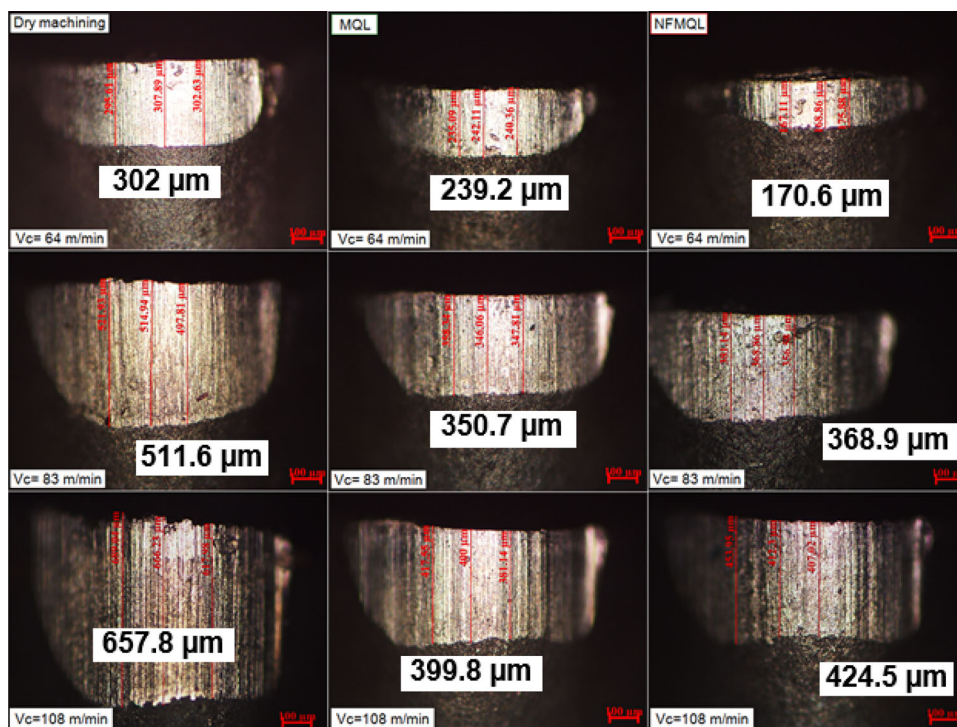




**Fig. 6** Details of tool wear modes as observed in worn-out insert ($V_c = 64$ m/min, dry condition)

cal affinity of Inconel 718 (toward tool materials, and binder) causes adhesion wear. Results of EDS analysis as depicted in Fig. 9 clearly infers the presence of main constituents of Inconel 718 (such as Ni, Cr, Nb, and Fe) within the adhered layer. As explained by Devillez et al. [43], in the sliding zone (area on the tool face over which chip starts to slide), at relatively lower pressure and temperature; unstable adhered layer is formed which is subsequently removed; while removal, it pulls off coating (if the coated tool is used), and substrate particles from the tool face. This results in formation of crater.

The voids over the tool face may be caused due to plucking off tool material during the removal of BUL. Voids may also be caused due to the defect (lack of compaction) incurred during tool manufacturing. Tiny chip fragments are found sticking onto the tool face due to their inadequate inertia to overcome frictional force at the tool-chip interface.

Tool wear mechanisms at $V_c = 83$ m/min, corresponding to dry, MQL, and NFMQL conditions (after 40 s machining), respectively, can be understood from Figs. 10, 11, and 12. Micrographs reveal different tool wear mechanisms: crater
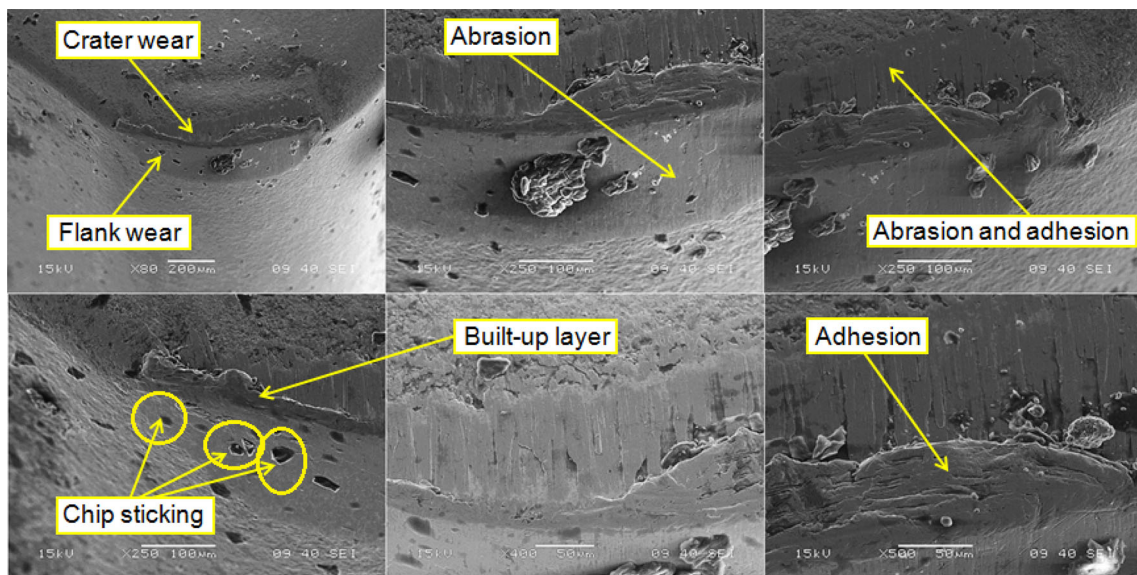
**Fig. 7** Details of tool wear modes as observed in worn-out insert ($V_c$ = 64 m/min, MQL condition)
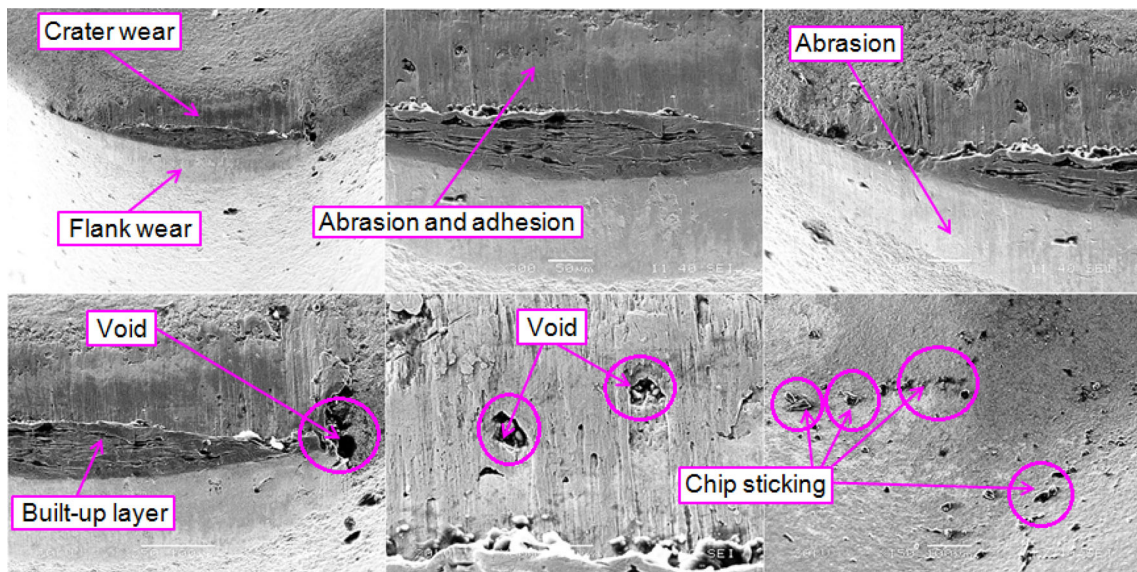


**Fig. 8** Details of tool wear modes as observed in worn-out insert ($V_c$ = 64 m/min, NFMQL condition)

wear, formation of BUL, abrasion, and adhesion. In addition, extreme cutting temperature, evolved under dry machining, leads to severe chip burning. On the contrary, under MQL, chip sticking and welding are experienced over tool face due to the lower cutting temperature generated. Under NFMQL, further reduction in cutting temperature limits the chips to be slicked/fused over tool face. At elevated pressure and temperature, atoms of work material may form bonding and fuse over the tool face. Residues of wear debris are adhered on tool flank face (under MQL and NFMQL). Tremendous cutting temperature results in chip burning and formation of metallic oxides of constituents of tool/work material. EDS

analysis result as provided in Fig. 13 exhibits residues of work elements along with oxygen in abundance.

Figures 14, 15, and 16 display tool wear mechanisms incurred at $V_c$ = 108 m/min (after 40 s machining duration), under dry, MQL, and NFMQL, respectively. Dominant wear mechanisms: abrasion, adhesion, chip sticking, etc. are observed irrespective of machining environments employed. Dry machining environment appears highly aggressive, affecting cutting tool through notch wear, chip fusion, chip welding, and chip burning. On the contrary, MQL and NFMQL restrict formation of notches as well as limit welding/burning of chips; however, the formation of BUL is experienced therein. In the case of NFMQL, in addition to
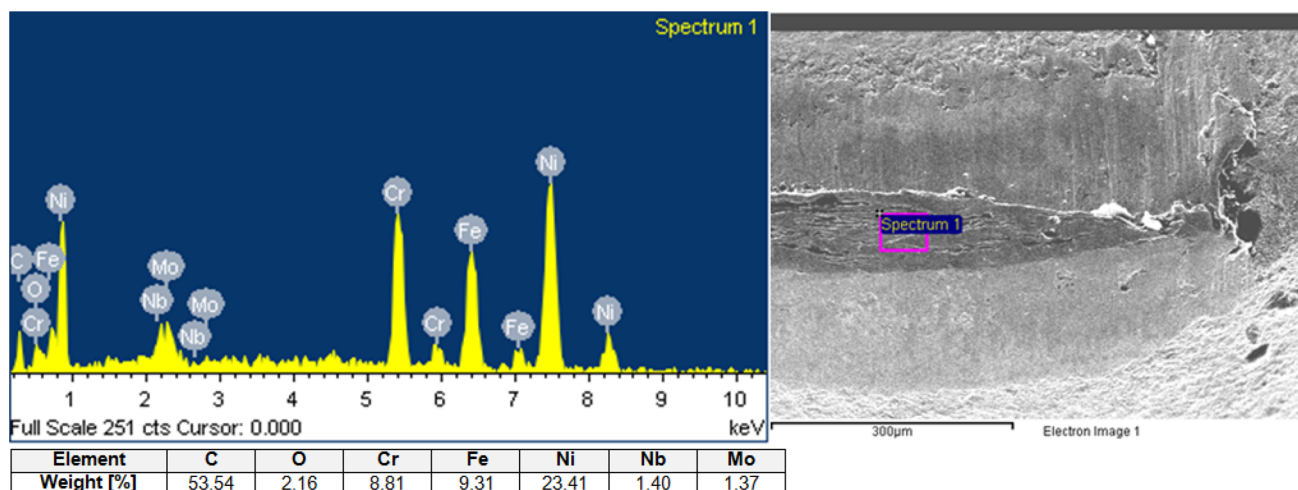
**Fig. 9** EDS analysis made on built-up-layer ($V_c$ = 64 m/min, NFMQL condition)
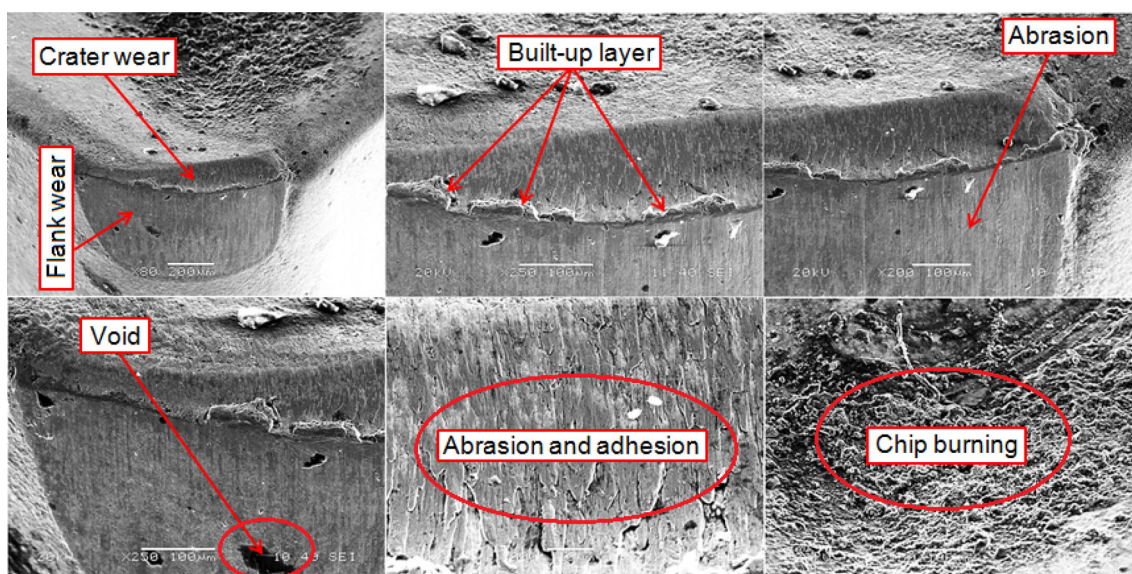


**Fig. 10** Details of tool wear modes as observed in worn-out insert ($V_c$ = 83 m/min, dry condition)

common tool wear mechanisms, the deposition of carbon particles is retrieved which may be due to intense shaking/vibration of tool at higher cutting speeds which causes splashing of oil from the cutting zone and settlement of MWCNTs over tool face. Combined effect of high cutting temperature, hot strength of work material, and presence of hard abrasive carbide particles within workpiece leads to the formation of notches along the depth-of-cut line [17]. As demonstrated by Kasim et al. [44], notch initiates with the formation of pits due to the repetition of cyclic loads. Such pits may further expand which leads chipping; and increased degree of chipping along with abrasion action results in the formation of long grooves on tool rake/flank face, close to the depth-of-cut line. This is called notch wear. High temperature and pressure, generated during machining, result in welding of chip segments over tool face [45]. EDS data

(as shown in Fig. 17) exhibit traces of carbon, in adequate proportion, confirming the deposition of MWCNTs (coming from nanofluid), along with relatively lower weight percentage of oxygen (as compared to EDS in Fig. 13). This reduces the chance of chip burning.

Micrographs are arranged in Figs. 18, 19, and 20 which depict details of tool wear mechanisms after 40 s machining at $V_c$ = 140 m/min, under different machining environments. In the case of dry machining (Fig. 18), prominent wear mechanisms involved are notch wear, adhesion, abrasion, crater formation, voids, chip fusion, chip sticking, and chip burning. On the other hand, Fig. 19 reveals that under MQL, due to improvement in overall machinability, tool wear is to somewhat restricted to tool chipping off before formation of notch; while, in the case of NFMQL (Fig. 20), tool edge chipping is not even noticed. This clearly indicates that NFMQL
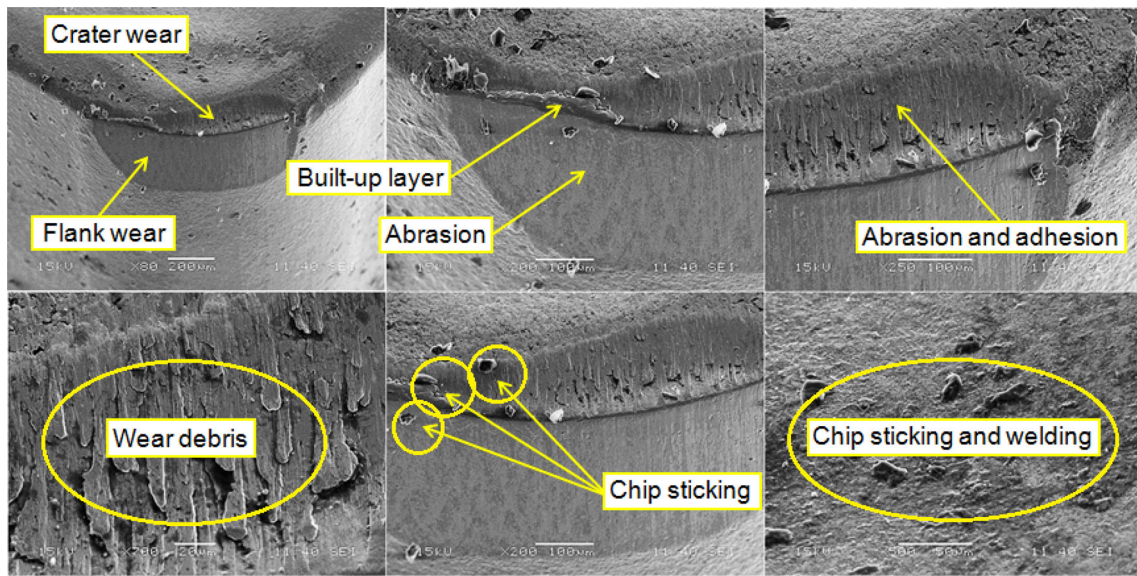
**Fig. 11** Details of tool wear modes as observed in worn-out insert ($V_c$ = 83 m/min, MQL condition)
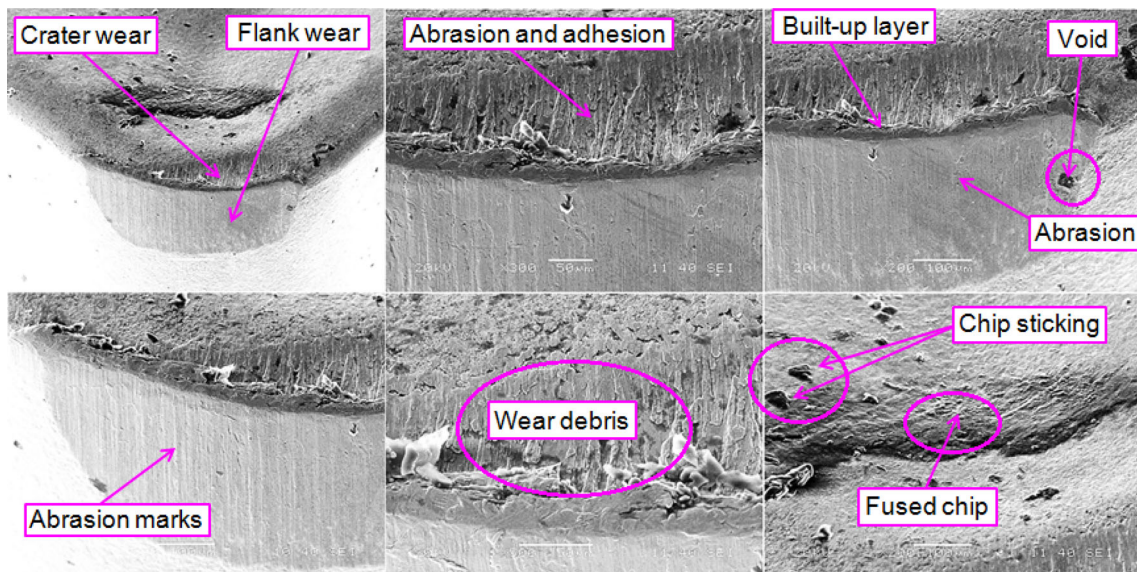


**Fig. 12** Details of tool wear modes as observed in worn-out insert ($V_c$ = 83 m/min, NFMQL condition)

outperforms conventional MQL so far as severity of notch wear is concerned.

XRD analysis carried out on worn-out tool-tip, operated at $V_c$ = 140 m/min, under NFMQL condition, detects new phases like $Fe_{0.928}O$, and $Ni_{2.9}Cr_{0.7}Fe_{0.36}$ in addition to WC peaks (Fig. 21). Formation of new phases, containing elements of work material (and oxides), provides a clear-cut indication of work material adhesion over tool face.

### 4.5 Chip Morphology

Chip morphology study provides a clear insight regarding work material deformation occurring in primary deforma-

tion zone. Cutting speed plays a significant role to influence work part thermal softening as well as rate of stain-hardening, which finally governs mechanisms of chip formation, especially, while machining of nickel-based superalloys. In the present work, mechanisms of chip formation along with chip morphological parameters are studied at varied cutting speeds under different cutting environments: dry, MQL, and NMQL, respectively.

When machining is executed under dry environment beyond $V_c$ = 108 m/min, light golden colored chips are obtained; and at the highest cutting speed, i.e., $V_c$ = 140 m/min, chips tend to be burnt, and color turns to brown after 33 s machining duration, due to excessive heat gen-
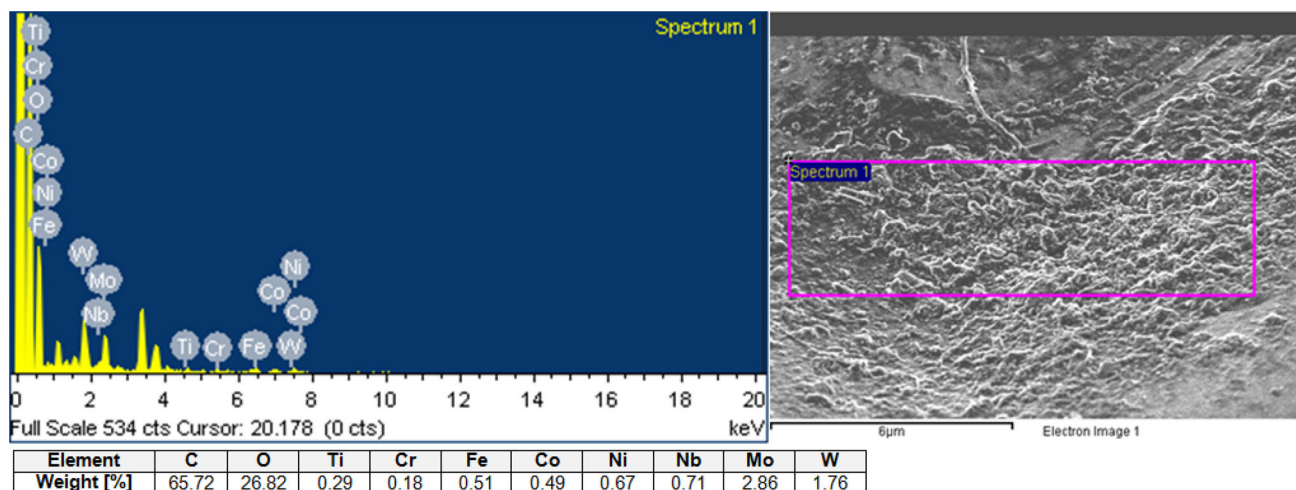
| Element | C | O | Ti | Cr | Fe | Co | Ni | Nb | Mo | W |
|---------|-----|-----|------|------|------|------|------|------|------|------|
| Weight [%] | 65.72 | 26.82 | 0.29 | 0.18 | 0.51 | 0.49 | 0.67 | 0.71 | 2.86 | 1.76 |

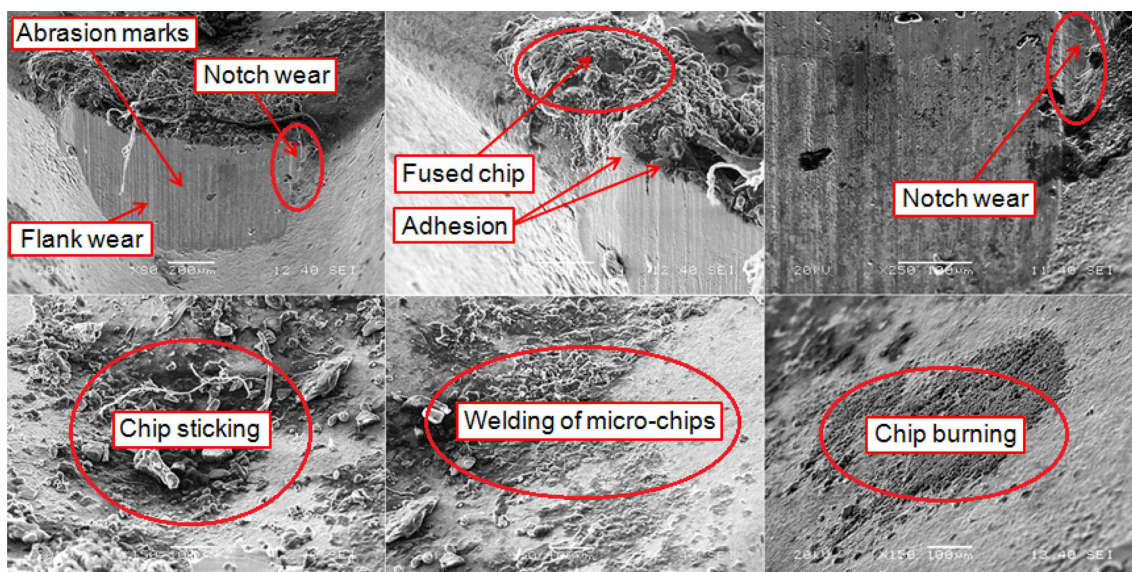Fig. 13 EDS analysis made on zone of oxidation over tool rake face ($V_c$ = 83 m/min, dry condition)



Fig. 14 Details of tool wear modes as observed in worn-out insert ($V_c$ = 108 m/min, dry condition)

eration at the highest cutting speed during dry machining (Fig. 22). On the other hand, while machining is done under MQL condition, light golden colored chips are observed at the highest cutting speed of $V_c$ = 140 m/min; and for NFMQL, the same is observed at $V_c$ = 140 m/min, after 35 s machining duration. During MQL machining, chips become golden in color only at the highest cutting speed due to proper penetration of cutting fluid into the cutting zone which enhances heat dissipation, and thus, results in huge temperature reduction at tool-chip interface. There is no trace of chip burning in the entire operation domain. Similar observation was reported by Gupta et al. [46]. Improved thermal conductivity and wettability of nanofluid enhance cooling capacity. NFMQL restricts the generation of golden colored chips up to 35 s machining duration at the highest cutting speed ($V_c$ = 140 m/min).

The helix angle (angle sustained by the axis about which chip curls, and the tangent to the chip surface of helical coiled chips) is reduced with increment in cutting speed, irrespective of cutting environments employed. A lesser degree of chip curling at higher cutting speeds can be explained by the lesser time that is available for the chip to curl, due to instantaneous cooling of chips as large surface comes in contact with ambient air. From Fig. 22, it is evident that the degree of chip curling is the least in the case of NFMQL, and the highest degree of chip curling is witnessed in dry machining.

According to Chetan et al. [9], due to the temperature gradient generated between free and sliding/back (underside) surface of chip, the chip acts as bimetallic-spring, resulting in the formation of curled chip. Excessive chip curling, as observed in dry machining, is due to the absence of coolant which results in high-temperature differential between chip's

**Fig. 15** Details of tool wear modes as observed in worn-out insert ($V_c = 108$ m/min, MQL condition)
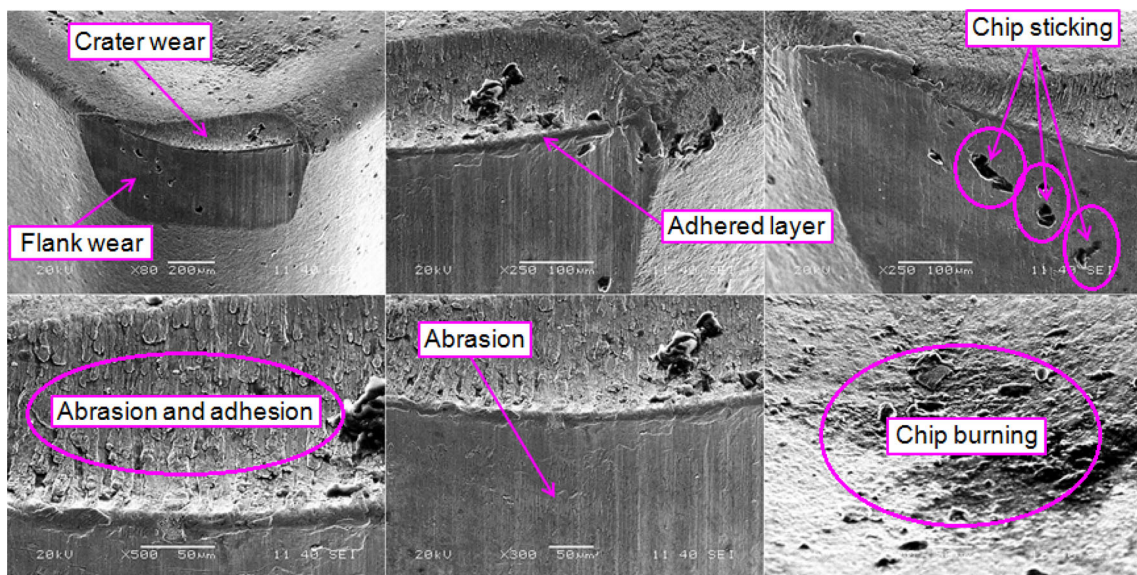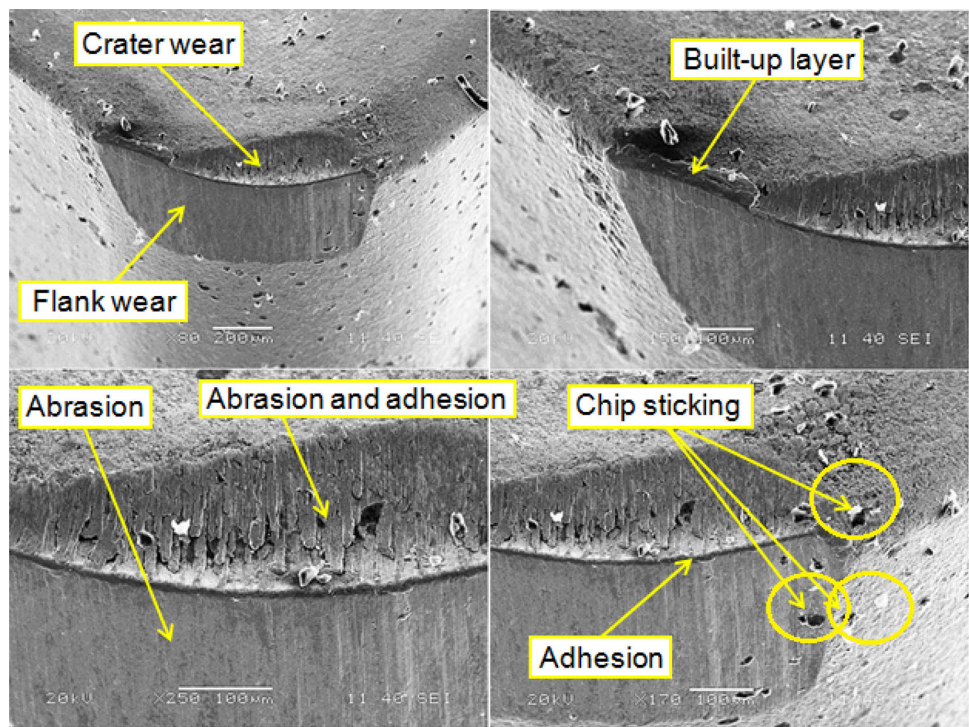




**Fig. 16** Details of tool wear modes as observed in worn-out insert ($V_c = 108$ m/min, NFMQL condition)

fee and sliding surface. On the other hand, minimal chip curling, as noticed under NFMQL machining, may be due to reduced contact angle, surface tension, and enhanced spreadability/wettability characteristics of nanofluid which ensures proper penetration of cutting fluids into the cutting zone. Effective penetration provides adequate cooling and lubrication, and thus, reduces temperature differential between chip's free, and sliding surface. In all experiments, serrated (segmented) or saw-toothed chip profile is obtained which

can be viewed from optical micrographs of the chip's cross-section.

According to Pawade and Joshi [47], the serrated type of chips is produced mainly due to thermal-assisted deformation at elevated cutting temperature, while machining of Inconel 718. Thermal-assisted deformation leads to initiation of cracks which propagates through the zone of primary deformation. Crack formation/propagation along with shear instability, caused due to thermoplastic deformation, leads to obvious chip serration. Dong et al. [48] also explained
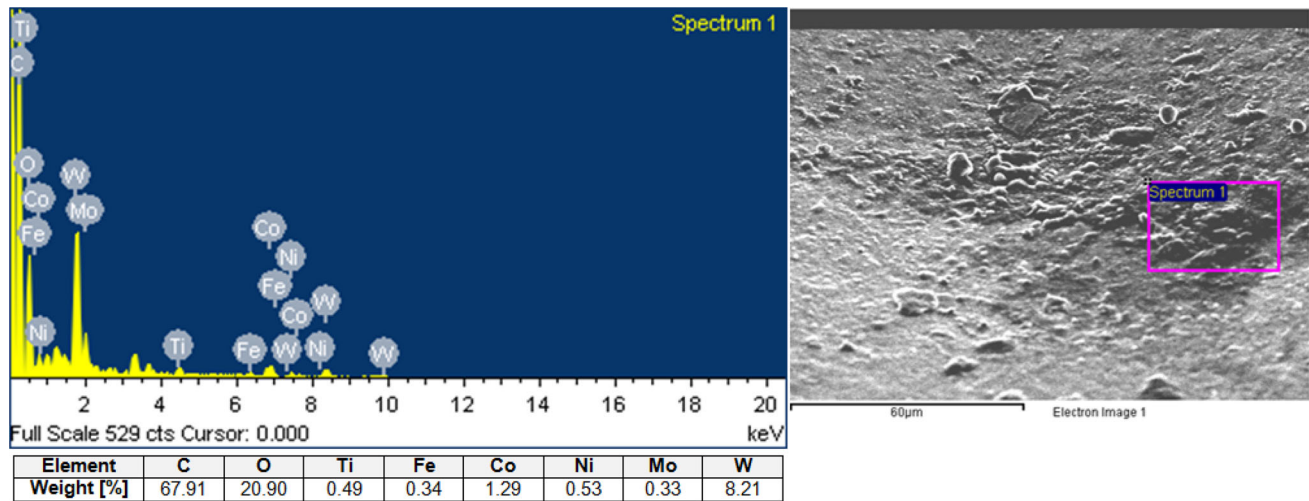
**Fig. 17** EDS analysis revealing carbon migration onto worn-out tool rake face ($V_c = 108$ m/min, NFMQL condition)

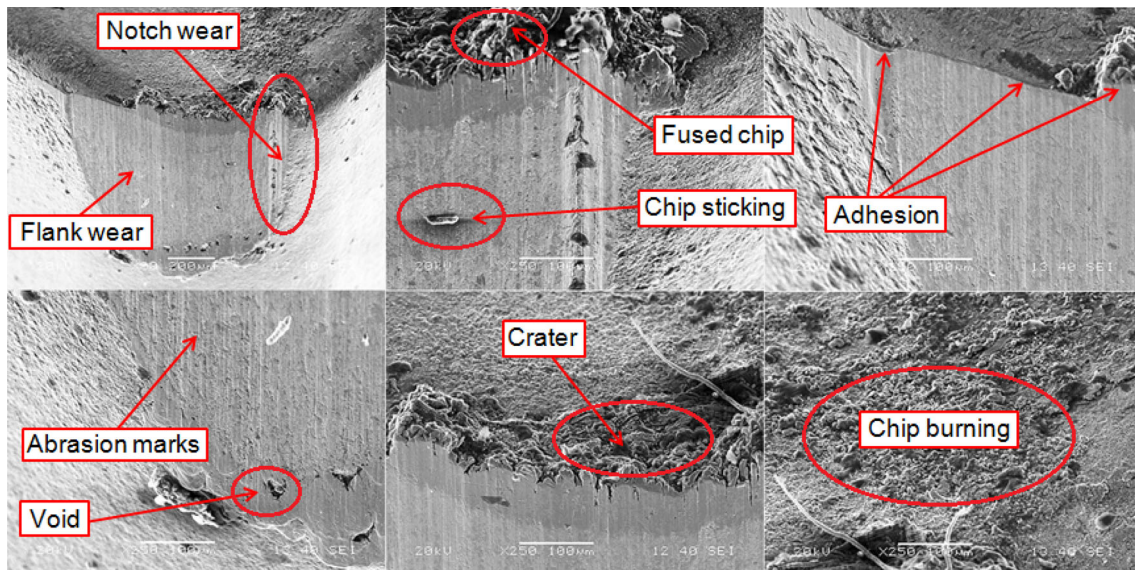| Element | C | O | Ti | Fe | Co | Ni | Mo | W |
|---------|------|------|------|------|------|------|------|------|
| Weight [%] | 67.91 | 20.90 | 0.49 | 0.34 | 1.29 | 0.53 | 0.33 | 8.21 |



**Fig. 18** Details of tool wear modes as observed in worn-out insert ($V_c = 140$ m/min, dry condition)

the mechanism of serrated chip formation during machining of Inconel 718. As compressive force within shear zone is increased, shear angle is gradually reduced. Under this circumstance, the thickness of shear plane is increased followed by transformation into three-dimensional (3D) zone called as *shear body*. At the end, adiabatic shear and cracks are developed at the chip's free surface which, in turn, cause the formation of a serrated chip profile. Further investigation on chip morphology is carried out on the basis of mean values of various chip micro-morphological parameters as described in Fig. 23.

Equivalent (or mean) chip thickness is one of the most important parameters in the purview of machinability assessment. Chip thickness has a significant effect on shear angle

and power consumption by the machine tool [49]. Equivalent chip thickness can be calculated as (Eq. 2) follows:

$$h_{\text{ch}} = h + \frac{H - h}{2} \tag{2}$$

$h_{\text{ch}}$ = mean/equivalent chip thickness ($\mu$m), $H$ = maximum chip height ($\mu$m), $h$ = minimum chip height ($\mu$m).

Friction at tool-chip interface, magnitude of machining forces, and tool wear are different reasons which cause varied effective chip thickness. At higher cutting speed, thinner chips are produced (Fig. 23a). At higher cutting speed, cutting edge rounding becomes more severe which leads to the reduced thickness of the effective deformed layer and, consequently, the formation of thin chips [50]. According to Ning et al. [51], at higher cutting speed, chips encounter higher shear localization due to the thermal softening of
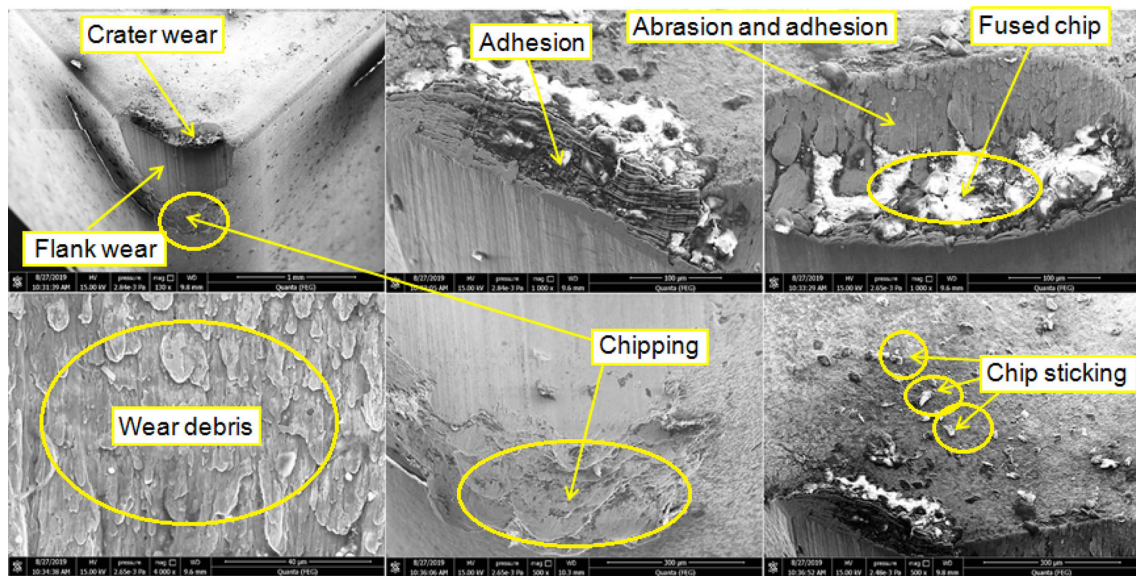
**Fig. 19** Details of tool wear modes as observed in worn-out insert ($V_c$ = 140 m/min, MQL condition)
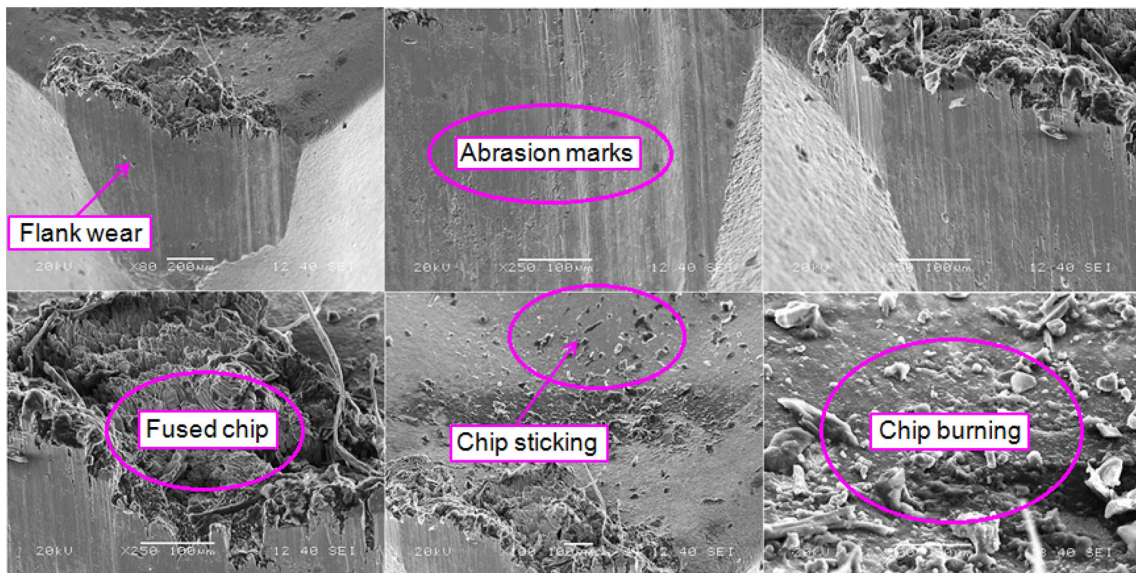


**Fig. 20** Details of tool wear modes as observed in worn-out insert ($V_c$ = 140 m/min, NFMQL condition)

work material owing to a higher temperature. This causes the formation of thin chips. From Fig. 23a, it is also observed that mean chip thickness is the highest under dry machining when compared to MQL and NFMQL. High temperature and pressure generated at cutting zone results in chip expansion, and thus, thick chips are produced under dry machining [9]. While machining under MQL/NFMQL, favorable cooling and lubrication reduce temperature and pressure at the cutting zone, which results in the reduction in mean chip thickness nearly 8.95–21.76% under MQL and 5.34–19.5% under NFMQL when compared to dry machining. Reduced mean chip thickness results in lower power consumption during machining [49]. Figure 4a also indicates a significant reduction in cutting force during MQL and NFMQL

machining as compared to dry cutting which implies lower power consumption. This also justifies the formation of thinner chips under MQL/NFMQL than dry machining.

The distance by which adjacent teeth of the serrated chip are apart is termed as saw-tooth distance (or pitch). It is also known as chip segmentation spacing. An increase in cutting speed causes shorter pitch as shown in Fig. 23b. A similar trend was also reported by Pawade and Joshi [47]. According to Ning et al. [51], at lower cutting speed, extrusion of the chip by tool rake face consumes much time, and tool-chip interface experiences higher friction. Significant plastic deformation of workpiece is incurred to chip's free end which leads to enlarged pitch. On the other hand, at higher cutting speed, tool rake face interacts with the chip for

🍃 Springer
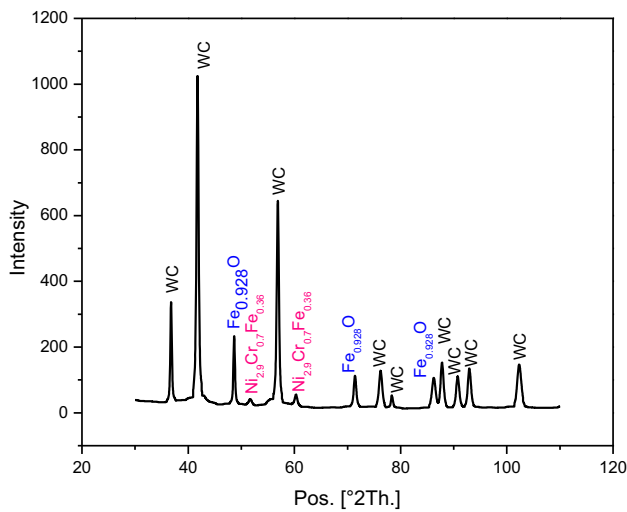
**Fig. 21** XRD results of worn-out tool-tip operated at $V_c = 140$ m/min under NFMQL

a short time duration; the frictional effect is also truncated at higher cutting speeds. This weakens chip extrusion and leads to incomplete plastic deformation; consequently, the pitch becomes shortened. It is witnessed that MQL and NFMQL conditions cause reduced pitch value. A similar result was published by Kaynak [18]. Reduction in pitch during MQL and NFMQL machining condition is due to favorable lubrication effect which reduces interfacial frictional coefficient and thus allows smooth flow of chips with high velocity. Chips experience less time while passing over tool rake face; and weaker chip extrusion leads to improper plastic deformation, and finally, reduced pitch.

Chip segmentation frequency can be defined as the number of saw-tooth generated per unit time while serrated chips are formed. Chip segmentation frequency (also called serration frequency) can be expressed as (Eq. 3) follows:

$$f_z = \frac{100 \times V_{chip}}{6 \times P_c} \tag{3}$$

$f_z$ = chip segmentation frequency (kHz), $V_{chip}$ = velocity of chip (m/min), $P_c$ = pitch of serrated chip (μm).

Applying condition for continuity or conservation of mass flow rate across the shear plane, chip velocity can be computed through Eqs. 4–5.

$$\rho_w \times f \times d \times V_c = \frac{(\rho_{chip} \times h_{ch} \times w_{chip} \times V_{chip})}{1000} \tag{4}$$

$\rho_w$ = density of work material (g/cc), $f$ = feed (mm/rev), $d$ = depth-of-cut (mm), $V_c$ = cutting velocity (m/min), $\rho_{chip}$ = density of chip (g/cc), $w_{chip}$ = width of chip (mm).

$$V_{Chip} = 1000 \times \frac{V_c \times f \times d}{h_{ch} \times w_{chip}} \tag{5}$$

With an increase in cutting speed, chip segmentation frequency is increased as seen in Fig. 23c. At higher cutting speed, friction at the tool-chip interface is reduced; however, higher cutting zone temperature leads to thermal softening of the workpiece. This in turn improves machinability causing frequent chip segmentation [50]. According to Palanisamy et al. [52], chips become more serrated (increased serration frequency) due to severe flank wear. While machining at higher cutting speeds, extreme cutting temperature leads to aggressive flank wear, and thus, increases chip serration frequency. In one reporting, it was explained that saw-tooth formation (or chip segmentation) is caused by fluctuating machining forces. In other words, chip serration frequency can be treated as an indicator of cutting force variation [53, 54].

It is also evidenced that serration frequency is increased in the case of MQL/NFMQL as compared to dry machining. This is due to the effect of superior lubrication effect (reduced friction) of cutting fluid. A comparative study between MQL and NFMQL reveals that chip serration frequency is higher for MQL at low cutting speeds, while for higher cutting speeds NFMQL corresponds to higher serration frequency, due to lesser value of pitch in consecutive speed ranges. At higher cutting speed, nanofluid develops strong *hydrodynamic tribo-film* over the tool face. Such *tribo-film* exerts a hydrodynamic force which tries to push chips away from the tool rake face. This enhances the possibility of chip segmentation (enhanced chip breakability).

Shear angle is the angle of the inclination of the shear plane with the direction of cutting velocity. It can be calculated as (Eq. 6) follows:

$$\tan \theta = \frac{\cos \gamma}{\left(\frac{h_{ch}}{h_{uc}}\right) - \sin \gamma} \tag{6}$$

$\theta$ = shear angle (°), $\gamma$ = rake angle (°), and $h_{uc}$ = uncut chip thickness (μm).

Here, uncut chip thickness is assumed to be nearly equal to the feed.

As cutting speed is increased, the shear angle is also increased, irrespective of machining environments employed (Fig. 23d). Similar trend was also observed by Kaynak et al. [55]. According to Bermingham et al. [56], an increase in cutting speed results in higher cutting zone temperature; the increased degree of work part thermal softening leads to increased shear angle. While machining is carried out under MQL/NFMQL, cutting force and friction are reduced as compared to dry machining, due to favorable cooling as well as lubrication effects. From (Eq. 5), it can be understood that lower mean chip thickness results in large shear angle, for constant machining parameters. This supports experimental results reflecting reduced chip thickness in the case of

**Fig. 22** Types of chips produced under different machining conditions: **a** $V_c = 64$ m/min, **b** $V_c = 83$ m/min, **c** $V_c = 108$ m/min, and **d** $V_c = 140$ m/min
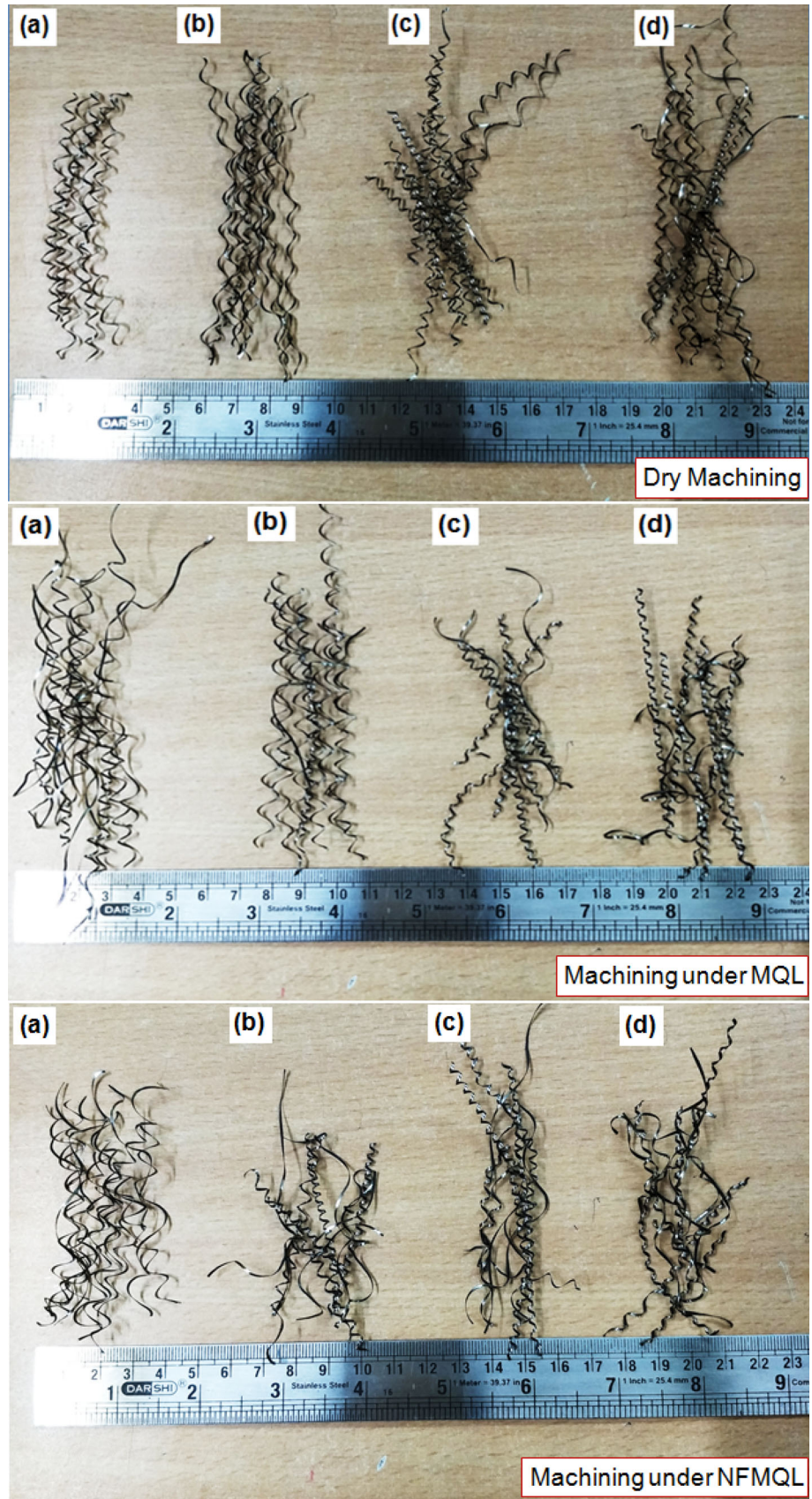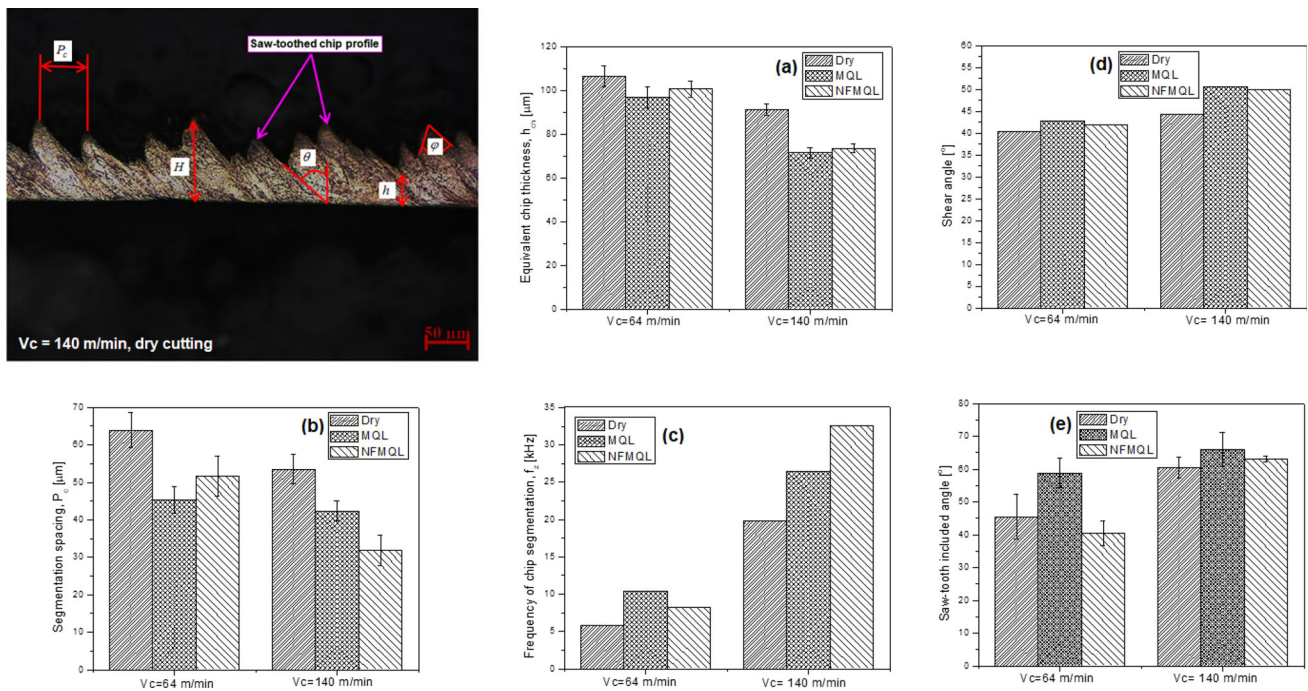
**Fig. 23** Effect of cutting speed on parameters of chip's micro-morphology

MQL/NFMQL than dry machining, under identical machining parameters condition.

The angle formed at top of saw-tooth by its sides, on the serrated chip profile, is known as saw-tooth included angle (or saw-tooth chip angle). The included angle indicates the tooth shape of the serrated chip profile. Included angle has a strong correlation with the fracture rate of work material toward generating chips [54]. Experimental results reveal that an increase in cutting speed results in increased saw-tooth included angle irrespective of machining environments maintained (Fig. 23e). This can be explained as follows: with an increase in cutting speed, the rate of deformation increases which causes higher stain-hardening of workpiece; thus, the wide included angle is obtained [50, 54]. Application of cutting fluids during MQL/NFMQL machining reduces cutting zone temperature which results in the reduced thermal-softening effect of the workpiece. Inadequate thermal softening of work material leads to a wider saw-tooth included angle.

Morphology of chip's free and back surfaces are described in Fig. 24. Severe friction tracks are detected on the chip's back surface produced under dry machining due to excessive friction. On the other hand, under MQL, the severity of such friction tracks appears relatively less. Under NFMQL, friction tracks are completely disappeared providing a shiny/smooth appearance of the chip's back surface. This is due to the excellent cooling, and lubrication effects of MWCNTs added nanofluid. Similar observation was also documented by Chetan et al. [9].

### 4.6 Chip Microhardness

Microhardness variation across the shear band is shown in Fig. 25. For a particular chip specimen, microhardness is measured at five distinct locations on three consecutive shear bands by using a micro-diamond imprint. Indentations are made with an impact load of 10 gf for 20 s dwell time. Intense shear localization, due to stain-hardening, results in increased microhardness which attains the maximum value at the midway of the shear band and tends to decline with increasing distance, away from the band. A similar kind of observation was also reported by Sun and Guo [57]. Chip microhardness is highly influenced by two counter-balancing factors, rate of strain-hardening which depends on strain rate, and thermal softening which depends on cutting zone temperature.

For constant cutting speed, the strain rate can be expressed as a function of shear angle and feed [58].

$$\dot{\varepsilon} = \frac{k \times \sin\theta \times \sin(45 + \theta)}{f \times \cos^2\theta} \tag{7}$$

$\dot{\varepsilon}$ = strain rate (s$^{-1}$), $k$ = constant (mm/s), $f$ = feed (mm/rev).

Calculated strain rate by using Eq. 7, corresponding to different machining environments at $V_c$ = 64 m/min (by using shear angle values as obtained from Eq. 6), it is understood that the strain rate is the maximum for MQL and minimal for dry machining. The minimal strain rate in dry machining is nearly 12% and 7% less as compared to MQL and NFMQL, respectively. This reveals that minimal strain-hardening in

**Fig. 24** Chip's back surface morphology at $V_c = 64$ m/min under **a** dry condition, **b** MQL, and **c** NFMQL
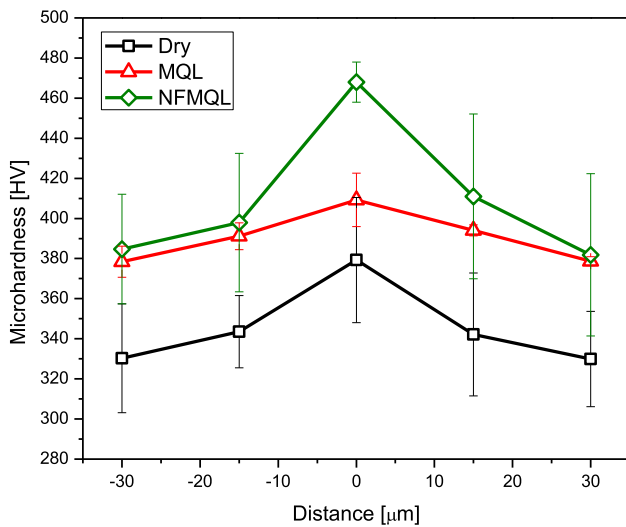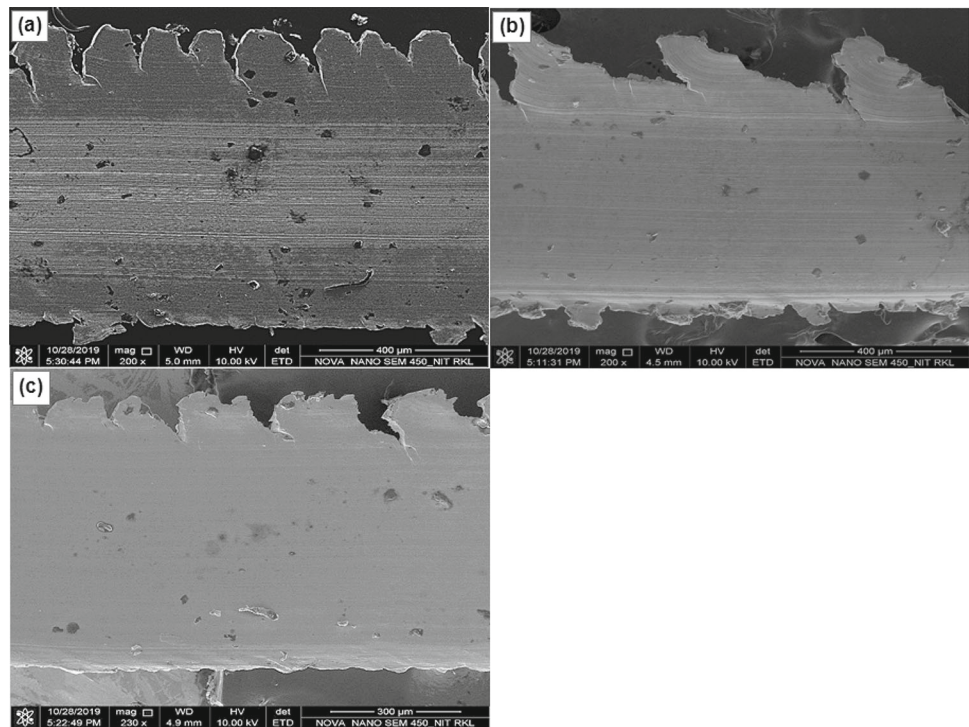




**Fig. 25** Microhardness distribution on both sides of the shear band: Chips produced at $V_c = 64$ m/min, under dry, MQL, and NFMQL conditions

extent of thermal softening. Between these two counter-balancing effects, thermal-softening effect dominates over strain-hardening effect in the case of MQL which leads to lower microhardness of chips when compared to NFMQL. Chips obtained under NFMQL correspond to 408.7 HV average microhardness; whereas, MQL and dry cutting cause average microhardness of chips 390.31 HV and 345 HV, respectively.

### 4.7 Machined Surface Roughness

Surface roughness of the machined work part is an indicator of the machined surface quality produced. Surface roughness is highly influenced by cutting parameters, tool geometry, machining environment, and composition of tool as well as workpiece.

Variation of surface roughness with respect to cutting speed is graphically presented in Fig. 26. Surface roughness is increased with increase in cutting speed for dry, MQL, and NFMQL. Increase in cutting speed leads to increase in flank wear width (as shown in Fig. 4d) which results in altered tool geometry. As a consequence, surface roughness is increased; or in other words, quality of the machined surface deteriorates. Surface roughness attains the maximum value for dry machining, and minimal value in the case of NFMQL. A similar trend was also reported by Yıldırım et al. [25]. MQL technique ensures adequate penetration of cutting fluid into the cutting zone which enhances fast heat transfer. Hence, reduction in cutting zone temperature is witnessed. Lubricity

dry condition is accompanied by enormous thermal softening due to maximum cutting temperature generated which is nearly 55% and 64% more than MQL and NFMQL, respectively. This leads to minimal microhardness of chips obtained under dry machining (Fig. 25).
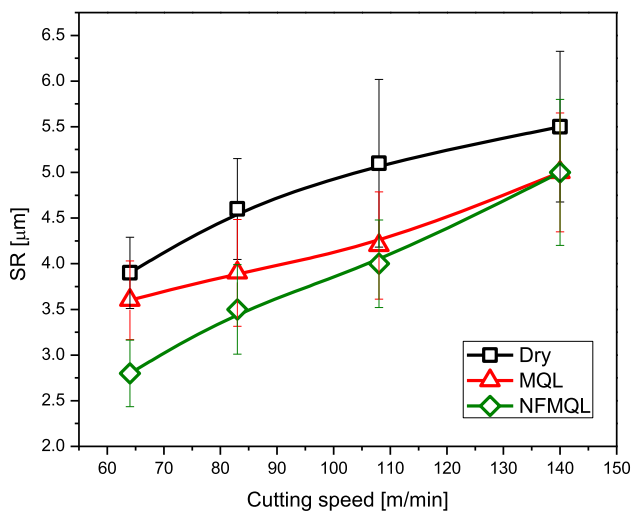
The strain rate for machining under MQL appears 5% more than NFMQL; on the other hand, cutting zone temperature in the case of MQL is nearly 21% more than NFMQL. Higher strain rate implies intense stain-hardening; simultaneously, higher cutting temperature leads to greater

**Fig. 26** Effects of cutting speed on surface roughness of the machined work part

property of cutting fluid reduces friction at tool-chip as well tool-work interfaces which results in reduced cutting force. Reduced cutting force ultimately leads to lower tool wear and better surface finish. Introduction of nano-particles into cutting fluid enhances wettability of the resultant cutting fluid. Larger area on cutting zone gets wetted. Improved thermal conductivity of nanofluid ensures efficient heat dissipation from the cutting zone. In addition to this, *roller-bearing* effect provided by MWCNTs contributes toward reduction in interfacial friction which leads to reduction in tool wear, and superior surface finish. Upon comparison on machined surface quality obtained under MQL and NFMQL at $V_c =$ 140 m/min, it is observed that the machined surface produced under NFMQL corresponds to a lesser extent of chip sticking, feed marks, side flow (common machining defects), etc. than conventional MQL.

In Fig. 25, high standard deviation of microhardness data is due to the presence of hard inclusions in Inconel 718 chips. Large standard deviation of surface roughness data (shown in Fig. 26) is due to non-uniform distribution of oxidized material, metal debris/tiny chip fragments stuck on the machined surface, smeared material, and material side flow which are known as machining induced surface irregularities. Additionally, the common sources of error including instrumental, environmental, procedural, and human may also influence deviation of experimental data from the mean value.

## 5 Conclusions

- As compared to dry machining, MQL/NFMQL conditions require lower cutting force, nearly 20% less in the case of MQL and 9–10% less for NFMQL, within selected experimental domain.

- MQL/NFMQL reduces tool-tip temperature significantly than dry machining. Under NFMQL, tool-tip experiences minimal temperature up to $V_c = 108$ m/min. It is estimated that maximum reduction in tool-tip temperature is nearly 60% for MQL and 67% for NFMQL with respect to dry machining.

- When compared to dry cutting environment, flank wear width is truncated significantly upon applying MQL/NFMQL technique. Minimal flank wear width is attributed to the tool insert under NFMQL up to $V_c = 83$ m/min. Beyond that, MQL outperforms NFMQL.

- Adhesion (formation of BUE, and BUL), abrasion, chip sticking, chip fusion (welding), chip burning, etc. are found prominently visible in worn-out tool inserts operated under dry and MQL conditions. Similar wear mechanisms are evidenced in the case of NFMQL excluding chip fusion/burning. At low cutting speed, tool insert, operated under dry condition, is affected by attrition wear. On the contrary, at high cutting speed, the formation of notch is traced near the tool insert cutting edge in the case of dry machining. Work material adhesion over worn-out tool face is confirmed through the formation of $Fe_{0.928}O$, and $Ni_{2.9}Cr_{0.7}Fe_{0.36}$.

- Serrated chip formation is incurred in all machining environments (dry, MQL, and NFMQL) under consideration. However, color of the chips depends on cutting velocity and machining environment employed.

- MQL and NFMQL produce thinner chips than dry machining. As compared to dry machining, MQL and NFMQL form closely spaced segmented teeth in the saw-toothed chip profile. Consequently, the frequency of chip segmentation is increased in the case of MQL as well as NFMQL than dry machining.

- Wider shear angle is attributed to MQL/NFMQL machining than dry cutting which indicates lower cutting force, and hence, lesser power consumption.

- In the case of dry machining, severe friction tracks are identified on chip's underside surface. On the other hand, friction tracks are not so much prominent for MQL. But relatively smoother and shinier underside surface (without any friction track) is attributed to the chips obtained under NFMQL. The dirtiest chip's underside surface is obtained under dry environment.

- Chip's adiabatic shear band corresponds to higher microhardness than adjacent locations. Chips produced under NFMQL exhibit higher average microhardness than MQL and dry environment.

- NFMQL offers better surface finish than dry machining, and conventional MQL.

**Fig. 27** Setup for MQL supply
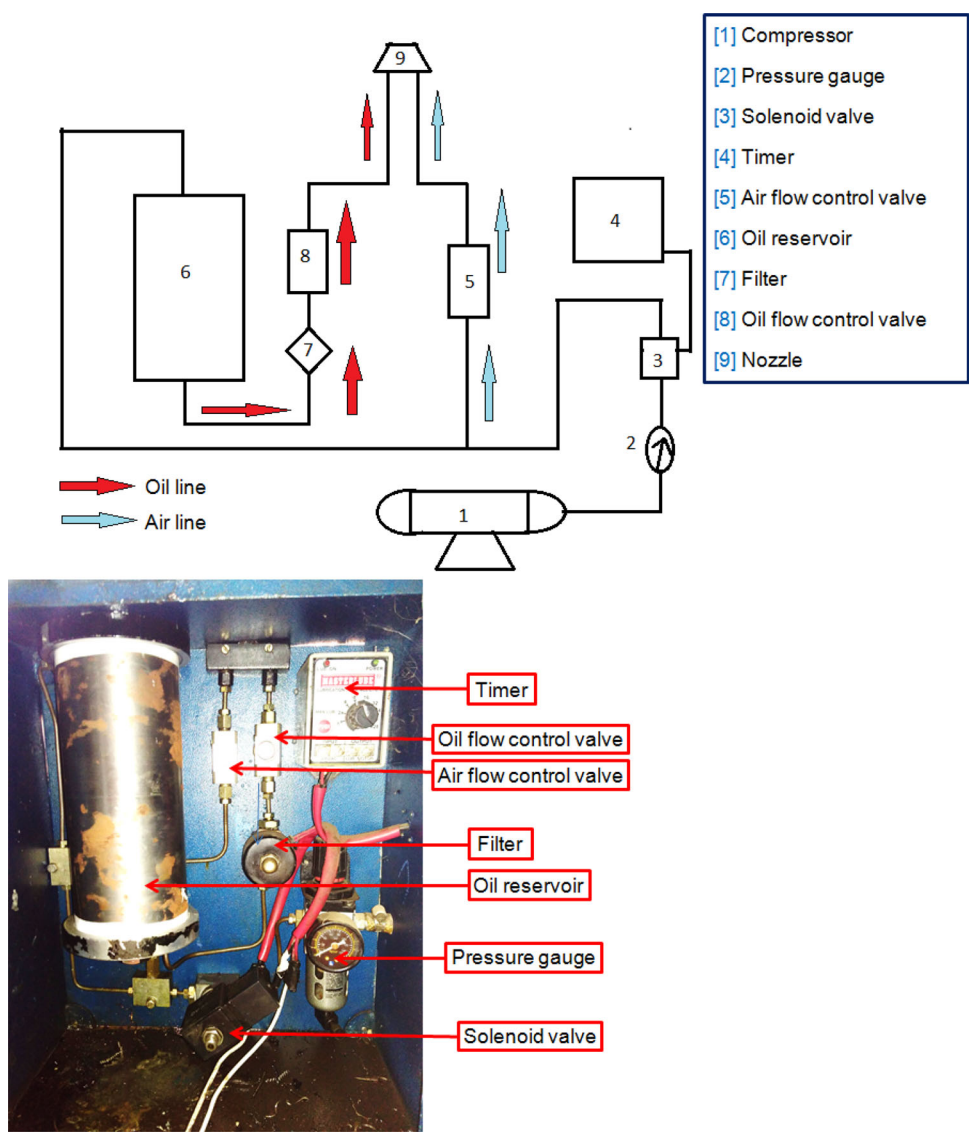


## 6 Future Scope

As furnished in Table 2, *as-received* MWCNTs contain < 2% ash, < 4000 mg/kg Fe, < 3500 mg/kg Al, and < 800 mg/kg Mo. It is believed that the level of constituents has a significant impact on the results. This aspect may be taken care of in future work. Though, literature seems almost scanty to deliver evidence of work carried out in this particular direction.

Feasibility of recycling the used cutting fluid and subsequent reuse need to be verified from the viewpoints of both operational and performance-related challenges. Looking into the operational aspect, collection of cutting fluid would be a challenging task, as cutting fluid is sprayed (as *mist*) onto the cutting zone, and even after collection, contaminates (fragmented chips/debris, dust) need to be removed from the cutting fluid by utilizing some kind of filtration

arrangements. If the working fluid is nanofluid, then complete separation of nano-additives from the debris/micro-chips is indeed a difficult task. While considering performance aspect of nanofluid, it is evidenced in the present work that nano-additives tend to get settled down at high machining speed which definitely alters nanofluid's composition. Thus, the reuse of nanofluid would significantly affect performance. In general, cutting fluid, once used during metal machining, is disposed/discarded.
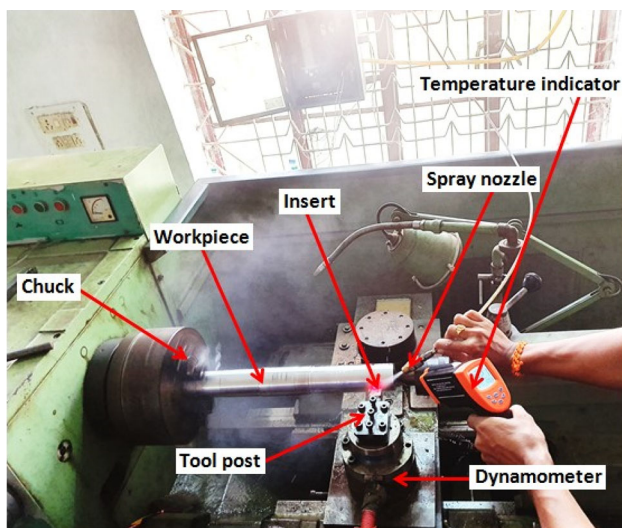
## Appendix

See Figs. 27 and 28.

**Fig. 28** Setup for machining experiment

# References

1. Zhuang, K.; Zhu, D.; Zhang, X.; Ding, H.: Notch wear prediction model in turning of Inconel 718 with ceramic tools considering the influence of work hardened layer. Wear **313**(1–2), 63–74 (2014)
2. Akca, E.; Gürsel, A.: A review on superalloys and IN718 nickel-based INCONEL superalloy. Period. Eng. Nat. Sci. **3**(1), 15–27 (2015)
3. Zhu, D.; Zhang, X.; Ding, H.: Tool wear characteristics in machining of nickel-based superalloys. Int. J. Mach. Tools Manuf **64**, 60–77 (2013)
4. Dudzinski, D.; Devillez, A.; Moufki, A.; Larrouquere, D.; Zerrouki, V.; Vigneau, J.: A review of developments towards dry and high speed machining of Inconel 718 alloy. Int. J. Mach. Tools Manuf **44**(4), 439–456 (2004)
5. Sharman, A.R.C.; Hughes, J.I.; Ridgway, K.: Surface integrity and tool life when turning Inconel 718 using ultra-high pressure and flood coolant systems. Proc. Inst. Mech. Eng. Part B J. Eng. Manuf. **222**(6), 653–664 (2008)
6. Kamata, Y.; Obikawa, T.: High speed MQL finish-turning of Inconel 718 with different coated tools. J. Mater. Process. Technol. **192**, 281–286 (2007)
7. Obikawa, T.; Kamata, Y.; Asano, Y.; Nakayama, K.; Otieno, A.W.: Micro-liter lubrication machining of Inconel 718. Int. J. Mach. Tools Manuf **48**(15), 1605–1612 (2008)
8. Shashidhara, Y.M.; Jayaram, S.R.: Vegetable oils as a potential cutting fluid—an evolution. Tribol. Int. **43**(5–6), 1073–1081 (2010)
9. Behera, C.B.C.; Ghosh, S.; Rao, P.V.: Application of nanofluids during minimum quantity lubrication: a case study in turning process. Tribol. Int. **101**, 234–246 (2016)
10. Yang, L.; Ji, W.; Zhang, Z.; Jin, X.: Thermal conductivity enhancement of water by adding graphene nano-sheets: consideration of particle loading and temperature effects. Int. Commun. Heat Mass Transf. **109**, 104353 (2019)
11. Xie, H.; Yu, W.; Chen, W.: MgO nanofluids: higher thermal conductivity and lower viscosity among ethylene glycol-based nanofluids containing oxide nanoparticles. J. Exp. Nanosci. **5**(5), 463–472 (2010)
12. Yang, Y.; Grulke, E.A.; Zhang, Z.G.; Wu, G.: Thermal and rheological properties of carbon nanotube-in-oil dispersions. J. Appl. Phys. **99**(11), 114307 (2006)
13. Choudhury, I.A.; El-Baradie, M.A.: Machining nickel base superalloys: Inconel 718. Proc. Inst. Mech. Eng. Part B J. Eng. Manuf. **212**(3), 195–206 (1998)
14. Rahman, M.; Seah, W.K.H.; Teo, T.T.: The machinability of Inconel 718. J. Mater. Process. Technol. **63**(1–3), 199–204 (1997)
15. Kitagawa, T.; Kubo, A.; Maekawa, K.: Temperature and wear of cutting tools in high-speed machining of Inconel 718 and Ti–6Al–6 V–2Sn. Wear **202**(2), 142–148 (1997)
16. Ezugwu, E.O.; Bonney, J.: Effect of high-pressure coolant supply when machining nickel-base, Inconel 718, alloy with coated carbide tools. J. Mater. Process. Technol. **153**, 1045–1050 (2004)
17. Altin, A.; Nalbant, M.; Taskesen, A.: The effects of cutting speed on tool wear and tool life when machining Inconel 718 with ceramic tools. Mater. Des. **28**(9), 2518–2522 (2007)
18. Kaynak, Y.: Evaluation of machining performance in cryogenic machining of Inconel 718 and comparison with dry and MQL machining. Int. J. Adv. Manuf. Technol. **72**(5–8), 919–933 (2014)
19. Zhang, S.; Li, J.F.; Wang, Y.W.: Tool life and cutting forces in end milling Inconel 718 under dry and minimum quantity cooling lubrication cutting conditions. J. Clean. Prod. **32**, 81–87 (2012)
20. Rahim, E.A.; Sasahara, H.: An analysis of surface integrity when drilling Inconel 718 using palm oil and synthetic ester under MQL condition. Mach. Sci. Technol. **15**(1), 76–90 (2011)
21. Behera, B.C.; Alemayehu, H.; Ghosh, S.; Rao, P.V.: A comparative study of recent lubri-coolant strategies for turning of Ni-based superalloy. J. Manuf. Process. **30**, 541–552 (2017)
22. Hegab, H.; Kishawy, H.A.: Towards sustainable machining of Inconel 718 using nano-fluid minimum quantity lubrication. J. Manuf. Mater. Process. **2**(3), 50 (2018). https://doi.org/10.3390/jmmp2030050
23. Hegab, H.; Umer, U.; Soliman, M.; Kishawy, H.A.: Effects of nano-cutting fluids on tool performance and chip morphology during machining Inconel 718. Int. J. Adv. Manuf. Technol. **96**(9–12), 3449–3458 (2018)
24. Vasu, V.; Reddy, G.P.K.: Effect of minimum quantity lubrication with $Al_2O_3$ nanoparticles on surface roughness, tool wear and temperature dissipation in machining Inconel 600 alloy. Proc. Inst. Mech. Eng. Part N J. Nanoeng. Nanosyst. **225**(1), 3–16 (2011)
25. Yıldırım, Ç.V.; Sarıkaya, M.; Kıvak, T.; Şirin, Ş.: The effect of addition of hBN nanoparticles to nanofluid-MQL on tool wear patterns, tool life, roughness and temperature in turning of Ni-based Inconel 625. Tribol. Int. **134**, 443–456 (2019)
26. Shuang, Y.; Mo, J.; Ding, S.: Experimental investigation on the performance and mechanism of graphene oxide nanofluids in turning Ti–6Al–4V. J. Manuf. Process. **43**(Part A), 164–174 (2019)
27. Shuang, Y.; Nan, L.; Solanki, S.; Mo, J.; Ding, S.: Effects of graphene oxide nanofluids on cutting temperature and force in machining Ti–6Al–4V. Int. J. Adv. Manuf. Technol. **103**, 1481–1495 (2019)
28. Wickramasinghe, K.C.; Perera, G.I.P.; Herath, H.M.C.M.: Formulation and performance evaluation of a novel coconut oil-based metalworking fluid. Mater. Manuf. Process. **32**(9), 1026–1033 (2017)
29. Perera, G.I.P.; Herath, H.M.C.M.; Perera, I.M.S.J.; Medagoda, M.G.H.M.M.P.: Investigation on white coconut oil to use as a metal working fluid during turning. Proc. Inst. Mech. Eng. Part B J. Eng. Manuf. **229**(1), 38–44 (2015)
30. Vardhaman, B.S.A.; Amarnath, M.; Jhodkar, D.; Ramkumar, J.; Chelladurai, H.; Roy, M.K.: Influence of coconut oil on tribological behavior of carbide cutting tool insert during turning operation. J. Braz. Soc. Mech. Sci. Eng. **40**, 450 (2018). https://doi.org/10.1007/s40430-018-1379-y
31. Vamsi Krishna, P.; Srikant, R.R.; Padmini, R.; Parakh, B.: Basic properties and performance of vegetable oil-based boric acid nanofluids in machining. In: Sathiyamoorthy, S., Caroline, B., Jayanthi, J. (eds.) Emerging Trends in Science, Engineering and

Technology. Lecture Notes in Mechanical EngineeringSpringer, Berlin (2012)

32. Padmini, R.; Vamsi Krishna, P.; Krishna Mohana Rao, G.: Effectiveness of vegetable oil based nanofluids as potential cutting fluids in turning AISI 1040 steel. Tribol. Int. **94**, 490–501 (2016)

33. Xavior, M.A.; Adithan, M.: Determining the influence of cutting fluids on tool wear and surface roughness during turning of AISI 304 austenitic stainless steel. J. Mater. Process. Technol. **209**, 900–909 (2009)

34. Lambarri, J.; Leunda, J.; Navas, V.G.; Soriano, C.; Sanz, C.: Microstructural and tensile characterization of Inconel 718 laser coatings for aeronautic components. Opt. Lasers Eng. **51**(7), 813–821 (2013)

35. Gugulothu, S.; Pasam, V.K.; Revuru, R.S.: Machining performance and sustainability of vegetable oil based nano cutting fluids in turning. In: Proceedings of 10th International Conference on Precision, Meso, Micro and Nano Engineering (COPEN 10) December 07–09. Indian Institute of Technology Madras, Chennai, India (2017)

36. Shankar, S.; Mohanraj, T.; Ponappa, K.: Influence of vegetable based cutting fluids on cutting force and vibration signature during milling of aluminium metal matrix composites. J. Tribol. **12**, 1–17 (2017)

37. Vardhaman B.S.A.; Amarnath, M.; Jhodkar, D.; Ramkumar, J.; Chelladurai, H.: Examining the role of cutting fluids in machining AISI 1040 steel using tungsten carbide insert under minimal quantity lubrication condition. In: Proceedings of 3rd International Conference on Advances in Engineering Sciences & Applied Mathematics (ICAESAM 2015), March 23–24, London, UK (2015)

38. Senevirathne, S.W.M.A.I.; Punchihewa, H K.G.; Kosgahakumbura, K.N.M.D.S.K.; Dissanayake, D.M.P.P.; Sahathevan, T.: Tool wear in machining AISI D2 steel with minimum quantity lubrication using alternative cutting fluids. In: Manufacturing and Industrial Engineering Symposium (MIES), Colombo, pp. 1–6 (2016)

39. Vamsi Krishna, P.; Srikant, R.R.; Nageswara Rao, D.: Experimental investigation on the performance of nanoboric acid suspensions in SAE-40 and coconut oil during turning of AISI 1040 steel. Int. J. Mach. Tools Manuf **50**(10), 911–916 (2010)

40. Pan, W.; Ding, S.; Mo, J.: Thermal characteristics in milling Ti6Al4V with polycrystalline diamond tools. Int. J. Adv. Manuf. Technol. **75**, 1077–1087 (2014)

41. Pan, W.; Kamaruddin, A.; Ding, S.; Mo, J.: Experimental investigation of end milling of titanium alloys with polycrystalline diamond tools. Proc. Inst. Mech. Eng. Part B J. Eng. Manuf. **228**(8), 832–844 (2014)

42. Akhtar, W.; Sun, J.; Sun, P.; Chen, W.; Saleem, Z.: Tool wear mechanisms in the machining of nickel based super-alloys: a review. Front. Mech. Eng. **9**(2), 106–119 (2014)

43. Devillez, A.; Schneider, F.; Dominiak, S.; Dudzinski, D.; Larrouquere, D.: Cutting forces and wear in dry machining of Inconel 718 with coated carbide tools. Wear **262**(7–8), 931–942 (2007)

44. Kasim, M.S.; Haron, C.C.; Ghani, J.A.; Sulaiman, M.A.; Yazid, M.Z.A.: Wear mechanism and notch wear location prediction model in ball nose end milling of Inconel 718. Wear **302**(1–2), 1171–1179 (2013)

45. Bhatt, A.; Attia, H.; Vargas, R.; Thomson, V.: Wear mechanisms of WC coated and uncoated tools in finish turning of Inconel 718. Tribol. Int. **43**(5–6), 1113–1121 (2010)

46. Gupta, M.; Pruncu, C.; Mia, M.; Singh, G.; Singh, S.; Prakash, C.; Sood, P.; Gill, H.: Machinability investigations of Inconel-800 super alloy under sustainable cooling conditions. Materials **11**(11), E2088 (2018). https://doi.org/10.3390/ma11112088

47. Pawade, R.S.; Joshi, S.S.: Mechanism of chip formation in high-speed turning of Inconel 718. Mach. Sci. Technol. **15**(1), 132–152 (2011)

48. Dong, G.; Zhaopeng, H.; Rongdi, H.; Yanli, C.; Muguthu, J.N.: Study of cutting deformation in machining nickel-based alloy Inconel 718. Int. J. Mach. Tools Manuf **51**(6), 520–527 (2011)

49. Ghosh, C.S.; Rao, P.V.: Environment friendly machining of Ni–Cr–Co based super alloy using different sustainable techniques. Mater. Manuf. Process. **31**(7), 852–859 (2016)

50. Thakur, A.; Gangopadhyay, S.: Evaluation of micro-features of chips of Inconel 825 during dry turning with uncoated and chemical vapour deposition multilayer coated tools. Proc. Inst. Mech. Eng. Part B J. Eng. Manuf. **232**(6), 979–994 (2018)

51. Ning, F.; Wang, F.; Jia, Z.; Ma, J.: Chip morphology and surface roughness in high-speed milling of nickel-based superalloy Inconel 718. Int. J. Mach. Mach. Mater. **15**(3–4), 285–299 (2014)

52. Palanisamy, S.; McDonald, S.D.; Dargusch, M.S.: Effects of coolant pressure on chip formation while turning Ti6Al4V alloy. Int. J. Mach. Tools Manuf **49**(9), 739–743 (2009)

53. Joshi, S.; Tewari, A.; Joshi, S.S.: Microstructural characterization of chip segmentation under different machining environments in orthogonal machining of Ti6Al4V. J. Eng. Mater. Technol. **137**(1), 011005 (2015)

54. Joshi, S.; Tewari, A.; Joshi, S.: Influence of preheating on chip segmentation and microstructure in orthogonal machining of Ti6Al4V. J. Manuf. Sci. Eng. **135**(6), 061017 (2013)

55. Kaynak, Y.; Gharibi, A.; Ozkutuk, M.: Experimental and numerical study of chip formation in orthogonal cutting of Ti-5553 alloy: the influence of cryogenic, MQL, and high pressure coolant supply. Int. J. Adv. Manuf. Technol. **94**(1–4), 1411–1428 (2018)

56. Bermingham, M.J.; Kirsch, J.; Sun, S.; Palanisamy, S.; Dargusch, M.S.: New observations on tool life, cutting forces and chip morphology in cryogenic machining Ti–6Al–4V. Int. J. Mach. Tools Manuf **51**(6), 500–511 (2011)

57. Sun, J.; Guo, Y.B.: A new multi-view approach to characterize 3D chip morphology and properties in end milling titanium Ti–6Al–4V. Int. J. Mach. Tools Manuf **48**(12–13), 1486–1494 (2008)

58. Jain, V.K.; Kumar, S.; Lal, G.K.: Effects of machining parameters on the microhardness of chips. J. Eng. Ind. **111**(3), 220–228 (1989)